

A Far Ultraviolet Analysis of the Stellar Populations in Six Elliptical and S0 Galaxies

Thomas M. Brown

Department of Physics and Astronomy, Johns Hopkins University
Charles and 34th Streets, Baltimore, MD 21218

Henry C. Ferguson

Space Telescope Science Institute
3700 San Martin Drive, Baltimore, MD 21218

Arthur F. Davidsen

Department of Physics and Astronomy, Johns Hopkins University
Charles and 34th Streets, Baltimore, MD 21218

and

Ben Dorman

Laboratory for Astronomy & Solar Physics, NASA/GSFC
Greenbelt, MD 20771

To appear in *The Astrophysical Journal*

ABSTRACT

We have analyzed the far-ultraviolet (FUV) spectra of six elliptical and S0 galaxies in order to characterize the stellar population that produces the ultraviolet flux in these galaxies. The spectra were obtained using the Hopkins Ultraviolet Telescope (HUT) during the Astro-2 mission aboard the Space Shuttle *Endeavour* in March 1995, and cover the spectral range from 820 to 1840 Å with a resolution of 3 Å. These data, together with the spectra of two galaxies observed with HUT on the Astro-1 mission, represent the only FUV spectra of early type galaxies that extend to the Lyman limit at 912 Å and therefore include the “turnover” in the spectral energy distribution below Lyman alpha.

Using an extensive new grid of LTE and non-LTE synthetic spectra which match the HUT resolution and cover the relevant parameter space of temperature and gravity, we have constructed synthetic spectral energy distributions by integrating over various predicted stellar evolutionary tracks for horizontal

branch stars and their progeny. When the computed models are compared with the HUT data, we find that models with supersolar metal abundances and helium best reproduce the flux across the entire HUT wavelength range, while those with subsolar Z & Y fit less well, partly because of a significant flux deficit shortward of 970 \AA in the models. High Z models are preferred because the contribution from the later, hotter, post-HB evolutionary stages makes up a higher fraction of the sub-Lyman α flux in these tracks. We find that AGB-Manqué evolution is required in all of the fits to the HUT spectra, suggesting that all of the galaxies have some subdwarf B star population. At any Z & Y , the model spectra that best match the HUT flux are dominated by stars evolving from a narrow range of envelope mass on the blue end of the horizontal branch.

The Astro-1 and Astro-2 data are also the first with the resolution and signal-to-noise needed to detect and measure absorption lines in the FUV spectra of elliptical galaxies, allowing a direct estimate of the abundances in the atmospheres of the stars that produce the UV flux. We find that most absorption features in the spectra are consistent with $Z = 0.1 Z_{\odot}$, significantly lower than the abundances implied by the best-fitting spectral energy distributions. However, given the strong observational and theoretical evidence for diffusion processes in the atmospheres of evolved stars, the observed atmospheric abundances may not reflect the interior abundances in the population producing the ultraviolet flux in elliptical galaxies.

Subject headings: galaxies: evolution — galaxies: abundances — galaxies: stellar content — ultraviolet: galaxies — ultraviolet: stars

1. INTRODUCTION

An understanding of the stellar populations in elliptical galaxies will shed light upon conflicting theories in cosmology, galactic evolution, and stellar evolution. However, 25 years after the initiation of space-based observations and the consequent extension of data into the ultraviolet (UV), there are still considerable uncertainties regarding the chemical composition in elliptical galaxies and the evolution of their stellar populations.

The spectra of elliptical galaxies and spiral galaxy bulges exhibit a strong upturn shortward of 2700 \AA , dubbed the “UV upturn.” Characterized by the $(m_{1550} - V)$ color, the UV upturn shows strong variation (ranging from 2.05–4.50 mag) in nearby quiescent

early-type galaxies (Burstein et al. 1988). The strength of the UV upturn is positively correlated with the strength of Mg_2 line absorption in the V band, in the sense that the $(m_{1550} - V)$ color is bluer at higher line strengths, opposite to the behavior of optical color indices (Burstein et al. 1988). Opposing theories have been devised to explain this correlation. In one camp, Lee (1994) and Park & Lee (1997) suggest that the UV flux originates in the low metallicity tail of an evolved stellar population with a wide metallicity distribution. In the other camp, several groups (Bressan, Chiosi, & Fagotto 1994; Greggio & Renzini 1990; Horch, Demarque, & Pinsonneault 1992) propose that metal-rich horizontal branch (HB) stars and their progeny are responsible for the UV flux. These different metallicity scenarios in turn argue for different ages for the stellar populations in these galaxies. Ages exceeding those of Galactic globular clusters are required in the Park & Lee (1997) model, while ages as low as 8 Gyr are allowed in the Bressan et al. (1994) model.

In these two scenarios, the EHB stars are drawn from either tail of the metallicity distribution. However, it is also possible, indeed perhaps more likely, that the EHB stars arise from progenitors near the peak of the metallicity distribution (cf. Dorman, O’Connell, & Rood 1995), but represent a relatively rare occurrence. Observations of a bimodal HB within the metal-rich open cluster NGC 6791 suggest that this might be the case (Liebert, Saffer, & Green 1994). If the same mechanism is at work in both the elliptical galaxies and in NGC 6791, the correlation of $(m_{1550} - V)$ with the global metallicity of the galaxy might indicate that this rare path of stellar evolution becomes less so at high metallicities.

1.1. Horizontal Branch Morphology

How can two diametrically opposed interpretations arise from the same observational data? The answer lies in the parameters that govern HB morphology, such as metallicity. In general, for stars of solar metallicity or less ($[\text{Fe}/\text{H}] < 0$), higher metallicities yield redder HBs and lower metallicities yield bluer HBs, i.e. bluer HBs have more stars on the blue side of the RR Lyrae instability strip, and redder HBs have more stars on the red side. Metallicity is the implied “first parameter” of HB morphology. In his spectrophotometry of 13 Milky Way globular clusters, Gregg (1994) gives an excellent observational example of the classical effect of metallicity on HB morphology; Lee, Demarque, & Zinn (1994) provide theoretical examples. However, it has been known for decades that other parameters affect HB morphology (cf. Lee et al. 1994 and references therein). In this way, the metallicity debate in elliptical galaxies is tied to the “second parameter” debate that has been raging in the study of globular clusters.

Helium abundance also plays an important role in the stellar structure of zero-age HB

(ZAHB) stars (Dorman 1992). These stars are characterized by a helium-rich core and a hydrogen-rich envelope. At the core/envelope boundary, the density ρ and mean molecular weight μ change such that ρ/μ is continuous. As the helium abundance (Y) in the envelope increases, the μ gradient across the core/envelope boundary decreases, which in turn decreases the temperature gradient across this boundary. Shallower temperature gradients produce higher shell temperatures, and the nuclear reactions in the hydrogen-burning shell are highly sensitive to the temperature. At the red end of the ZAHB, the shell luminosity in these massive envelopes makes a significant contribution to the total luminosity, and so an increase in temperature results in a significant increase in the total luminosity, but does not change the envelope structure significantly. At the blue end of the ZAHB, the shell luminosity in these less massive envelopes makes a smaller contribution to the total luminosity, and so the total luminosity does not change significantly with increasing temperature, but the envelope structure does. Thus, an increase in Y on the blue end of the ZAHB significantly increases T_{eff} and slightly increases the luminosity, while an increase in Y on the red end of the ZAHB significantly increases the luminosity and slightly increases T_{eff} . Across the entire ZAHB, an increase in Y increases the rate of nuclear reactions, resulting in more rapid consumption of the envelope.

Lee et al. (1994) argue that age is the second parameter driving HB morphology (see also Sarajedini, Lee, & Lee 1995). They also investigate the role of He abundance, CNO/Fe abundance ratio, and core rotation, but rule out these latter candidates for the second parameter because of conflicts with observations. Lee et al. (1994) find that age variations of several Gyr can produce dramatic differences in HB morphology, in the sense that young HBs (age = 11–12 Gyr) tend to be red, while older HBs (age = 15–16 Gyr) tend to be blue. This is because the mass of a red giant at the helium flash decreases as the age of a stellar population increases, which in turn decreases the mean mass of the HB stars (Lee et al. 1994 and references therein). Although this scenario is true in any given system, it must be stressed that when comparing different populations, the total mass loss on the red giant branch (RGB) may not have the same mean value and dispersion, and thus differences in HB morphology cannot necessarily be attributed to differences in age alone. When more than one parameter drives the HB mass distribution, it may be difficult to separate age from these other effects.

For an HB with a single metallicity, the envelope mass (M_{env}) determines the color location of stars on the HB. According to theory, stars with lower envelope mass are bluer (hotter) and stars with higher envelope mass are redder (cooler). Stars evolving off the HB at core helium exhaustion will then follow one of three different evolutionary scenarios, again depending upon the envelope mass. Dorman, Rood, & O’Connell (1993, hereafter DRO93) explain these evolutionary scenarios in detail; we will briefly summarize them here.

The first scenario occurs for an HB star with $M_{env} \gtrsim 0.07 M_{\odot}$ (in the case of solar Z and Y). Such a star evolves along the asymptotic giant branch (AGB), and after reaching the thermally pulsing (TP) stage, much of the envelope is removed and the star no longer sustains a deep convective exterior. At this point it evolves rapidly to higher temperatures at fixed luminosity, and then fades along the white dwarf (WD) cooling track. An example of a classical post-asymptotic giant branch (PAGB) evolutionary track (Vassiliadis & Wood 1994) is given in Fig. 1, along with the integrated far-ultraviolet (FUV) spectrum of a population of stars entering that track at the rate of one star per year. An AGB path that might precede the PAGB evolution is also shown (DRO93), but this cool, red portion of the evolution (from HB to TP) makes a negligible contribution to the integrated FUV luminosity in the HUT wavelength range.

The second scenario occurs if an HB star has enough envelope mass to reach the AGB, but not enough to maintain a convective exterior all the way to the TP stage ($0.03 M_{\odot} \lesssim M_{env} \lesssim 0.07 M_{\odot}$ for $Y = Y_{\odot}$ and $Z = Z_{\odot}$). These stars, dubbed post-early AGB (PEAGB; Brocato et al. 1990), evolve away from the AGB before reaching the TP stage, moving to higher temperatures at a constant luminosity which is less than that in the PAGB scenario. Because of the lower luminosity, and because models with lower envelope masses leave the AGB with more remaining hydrogen fuel, the PEAGB stars have longer lifetimes. Thus they emit more UV light over those lifetimes, as compared to the stars following the PAGB tracks. Fig. 1 shows an example of PEAGB evolution (DRO93) and the corresponding FUV luminosity. This particular PEAGB track exhibits helium shell flash TP “loops” which take place on the AGB if the envelope is more than a few hundredths of a solar mass. Although they are dramatic in the HR diagram, these short-lived features do not significantly alter the integrated spectrum.

The third scenario occurs for those HB stars with such small envelope masses ($M_{env} \lesssim 0.03 M_{\odot}$ for $Y = Y_{\odot}$ and $Z = Z_{\odot}$) that they are unable ever to develop deep outer convection zones, and thus are unable to reach the AGB at all. In the shell burning phase they are referred to as AGB-Manqué (AGBM) stars, and they spend $\sim 10^7$ yr at relatively high luminosity ($\sim 100 L_{\odot}$) and high temperature ($T_{\text{eff}} > 30,000$ K), after which they evolve directly to the WD cooling track. The amount of FUV light emitted from AGBM stars is much higher than that emitted from PAGB or PEAGB stars, as shown in Fig. 1, again due to their longer evolutionary time scales. Following the nomenclature of DRO93, we will use the term extreme HB (EHB) for those HB stars that evolve along PEAGB or AGBM evolutionary paths.

The different evolutionary paths a star may follow after leaving the HB are affected by the metallicity and helium abundance of the star. By itself, the envelope opacity at high Z

has a tendency to “damp down” the hydrogen burning shell, so that high-metallicity stars are fainter (Dorman 1992). It is usually supposed that enhanced metal abundance is seen in stellar populations accompanied with increases in the helium fraction, according to a simple linear formula: $\Delta Y/\Delta Z = \text{constant}$. Values for this constant are, however, determined from observations close to $Z = 0$ rather than $Z = Z_{\odot}$, since what is often sought is the primordial helium abundance for cosmological studies. There is little information about the helium abundance of metal-rich populations and the subject is quite controversial (see Dorman et al. 1995 and references therein; for a recent study, see Minniti 1995). For high He envelope abundance ($Y \gtrsim 0.40$), the envelope is consumed at a higher rate, because the hydrogen shell burns at higher temperatures (Dorman 1992; Sweigart & Gross 1976). The result is that more stars, with a greater range of envelope mass on the HB, will follow the PEAGB and AGBM paths (Fagotto et al. 1994c; DRO93). It must be stressed that it is the high *absolute* value of the helium abundance that causes this effect (and not the increase in Z).

High metallicity might affect the mass loss processes on the RGB. Compared to metal-poor RGB stars, metal-rich RGB stars have lower masses and larger radii at the same luminosity, and therefore lower surface gravities, which may in turn increase the rate of mass loss on the RGB (Horch et al. 1992 and references therein). With greater mass loss, more stars will arrive on the EHB. We note that although the increase of mass loss with increasing metallicity is certainly plausible, the effect remains unsubstantiated by theory or observations.

Once we understand the different physical parameters driving HB morphology, we may see how two different interpretations can arise for the correlation between Mg_2 strength and UV upturn strength. Arguing for the case of high metallicity, Bressan et al. (1994) say that more massive galaxies have higher mean and *maximum* metallicity, and thus — assuming Y also becomes high for high Z — more stars have a high enough metallicity to follow the evolutionary paths of the PEAGB and AGBM stars. Taking the opposing view, Lee (1994) argues that more massive galaxies have higher mean metallicity and are *older* than less massive galaxies, and thus whatever metal-poor fraction there is in the stellar population will have bluer HBs. Measurements of FUV line strengths have been proposed as sensitive tests of the models by both camps (see also Yi et al. 1995). In the Park & Lee (1997) model, one might expect to observe weak C IV and Si IV features anticorrelated with $(m_{1550} - V)$. In the metal-rich scenario, one might expect strong lines and a positive correlation with $(m_{1550} - V)$.

The different metallicity scenarios have important implications for the ages of elliptical galaxies and in turn the age of the Universe. Bressan et al. (1994) demonstrated that in

the high- Z – high- Y scheme, the onset of UV excess serves as an age probe, since it is the most rapidly evolving feature in the spectrum of an old elliptical galaxy. In their example, Bressan et al. (1994) show that the onset of UV excess occurs in the galaxy rest frame at an age of 7.6×10^9 yr. In the low-metallicity scheme, Park & Lee (1997) claim that giant elliptical galaxies must be at least 3 Gyr older than our own Galaxy, implying the lower limit to the age of the Universe must be 19 Gyr. Both models assume a Gaussian mass dispersion and either a Reimers (1975) mass loss law or fixed mass loss. The ages and metallicities at which the UV upturn begins to appear are unfortunately quite sensitive to these assumptions and to the parameters. The production of hot HB stars in the globular clusters and in the Galactic field is not easily described by a simple function, as we do not know how to characterize mass loss in stars. The UV upturn therefore has little value as an age indicator until the physics driving the phenomenon is understood.

In contrast, Dorman et al. (1995) argue that the size of the population of EHB stars — i.e., the fraction of all HB stars in the galaxy that are UV-bright — is the only sure deduction that can be made from the FUV radiation. They estimate, by using broadband colors derived from simple models of all evolutionary phases, that the blue FUV sources must have EHB fractions reaching $\sim 20\%$ of the HB population, a result only weakly dependent on the Z –abundance of the models. They argue that such a fraction is not a “trace population.” Instead, it is more plausible that the UV flux is produced by a significant minority of the dominant population, comprised of stars which have undergone higher mass loss than their red HB counterparts. The reason for the UV-Mg₂ correlation remains unknown, but may be explained by an increase in the likelihood of high mass loss in more metal-rich (or, at least, α –enhanced) stellar populations. In this picture there is no way to relate the FUV radiation to galaxy age, until mass loss in HB stars is better understood. In addition, the UV upturn is correlated with the velocity dispersion (σ_v), and although the correlation between ($m_{1550} - V$) and Mg₂ index is tighter than that between ($m_{1550} - V$) and σ_v (Burstein et al. 1988), it is not yet confirmed that the underlying correlation (i.e. causal relationship) is with abundance.

Because of the great uncertainties in the physical mechanisms responsible for the production of EHB stars, we have chosen in this paper to look at the constraints provided by the UV spectra themselves, with only very broad constraints on the overall stellar populations in the galaxies. Our conclusions are thus independent of any particular model of elliptical galaxy evolution. The limitation of this approach is that without a model there is no straightforward way to specify the distribution of stars on the zero-age HB. This would be a serious problem if there were a wide variety of FUV spectral energy distributions for normal elliptical galaxies. However, observations indicate that E galaxy FUV spectra are remarkably uniform (Burstein et al. 1988; Brown, Ferguson, & Davidsen 1995) and

consistent with a highly bimodal HB distribution (Ferguson 1994). Thus, for most purposes we can model the hot stellar population with only two evolutionary tracks, one for a PAGB star and one for an EHB star. We then adjust M_{env} for the EHB star and the fraction of the population in each type of star to achieve the best fit. In §4.4 we discuss the effect of relaxing this assumption of extreme bimodality.

1.2. Abundance Anomalies in Evolved Stars

It is not a straightforward exercise to determine the abundances in the stellar populations producing the UV light from elliptical galaxies. This is because the UV absorption line strengths in the spectra of evolved stars do not provide a direct measure of their inherent abundances. Numerous observations of HB stars and their progeny in our own Galaxy show that these stars exhibit abundance anomalies (see Saffer & Liebert 1995 and references therein). Helium is usually underabundant in sdB stars while overabundant in sdO stars. Carbon and silicon are usually underabundant in both sdB and sdO stars, while the nitrogen abundance usually appears normal in both classes (Saffer & Liebert 1995; Lamontagne, Wesemael, & Fontaine 1987; Michaud, Vauclair, & Vauclair 1983). The FUV spectra of evolved stars observed with HUT show absorption lines that are markedly different from solar abundances or even scaled solar abundances (Brown, Ferguson, & Davidsen 1996).

These abundance anomalies can be partly explained by models of diffusion processes in evolved stars, which demonstrate that abundances can be greatly enhanced or diminished through chemical separation in the stellar envelope and atmosphere. Individual elements can either levitate or sink in the outer layers of a star, depending upon which force has a stronger effect on each element: gravity (g) or radiative acceleration (g_{rad}). In theory, the tendency is for heavy elements to sink in cooler stars, and for these elements to levitate in hotter stars. If g_{rad} is larger than g , an element will be radiatively supported and it accumulates in the atmosphere, increasing line saturation, which in turn will decrease g_{rad} , until an equilibrium can be reached between g and g_{rad} (Bergeron et al. 1988). If g_{rad} is less than g , the element will sink into the star. However, the resulting abundance decrease may or may not lead to an increase in the local value of g_{rad} , depending upon whether or not the lines were originally saturated or unsaturated. Thus, an equilibrium between g and g_{rad} may or may not be reached (Bergeron et al. 1988). Michaud et al. (1983) demonstrated that if the abundances of C, N, O, Ca, and Fe are all assumed to be originally at 1/200 solar abundance, one can achieve abundance enhancements of three orders of magnitude through diffusion on the timescale of 10^8 yr. Unfortunately, diffusion theory has not reached

the level of accuracy needed to predict reliably the effects observed in evolved stars. For example, Bergeron et al. (1988) calculated three models with effective temperatures of 20,000 K, 35,000 K, and 50,000 K, and with respective gravities of $\log g = 5.0, 5.5,$ and 6.0 , all originally at solar abundance. They found that while the nitrogen abundance was at approximately solar abundance for all models, agreeing with observations, the behavior of carbon and silicon did not agree with observed trends. In the models, carbon was underabundant and increasing with T_{eff} , yet observations show that the carbon abundance seems to decrease with increasing T_{eff} (Bergeron et al. 1988 and references therein). Silicon was predicted to be between 0.1 and 1 of the solar value, but silicon deficiencies by factors of 10^4 – 10^5 are observed for these stars. Such discrepancies might point to other processes at work, such as a weak stellar wind (Bergeron et al. 1988). The bottom line is that these diffusion processes greatly complicate an absorption line analysis of an evolved population, and the strengths of the absorption lines are unlikely to reflect the inherent abundance of the population. Since the stronger metallic lines may well be saturated in stellar envelopes with very high abundances, metals in these envelopes may not be radiatively supported, allowing them to sink into the star. At the other extreme, very low abundances can be enhanced by orders of magnitude. Thus, diffusion processes tend to enhance low intrinsic abundances and diminish high intrinsic abundances.

In the elliptical galaxies, line analysis is further complicated by the fact that the spectra represent composite systems with components that cover a range in temperature and gravity, which in turn affect line strengths just as abundance does. Furthermore, in the FUV, the density of lines is so large that only the very strongest lines will be clearly distinct in these composite spectra.

With all of these complications in mind, an absorption line analysis alone will not answer the metallicity debate; we must look to the shape of the UV continuum as well. The shape of the continuum reflects the composite nature of these galaxies which no single temperature stellar model may duplicate (Brown et al. 1995), and thus reflects the evolutionary paths of the individual stars in the composite model. In this study, we use the stellar evolutionary models of DRO93, Bressan et al. (1993), and Fagotto et al. (1994a, 1994b, 1994c) to construct synthetic spectra for model stellar populations. The individual synthetic spectra which comprise the composite models are from the grids of Brown et al. (1996) and Kurucz (1992), for $T_{\text{eff}} \geq 10,000$ K and $T_{\text{eff}} < 10,000$ K respectively. The composite models which best fit the elliptical galaxy spectra draw the bulk of their flux from stars in the range $15,000 \text{ K} \leq T_{\text{eff}} \leq 30,000 \text{ K}$.

2. OBSERVATIONS

In March of 1995, the Hopkins Ultraviolet Telescope (HUT) was flown aboard the Space Shuttle *Endeavour* during the Astro-2 mission. It collected FUV spectra of six elliptical and S0 galaxies; these observations are summarized in Table 1. Together with the spectra of two galaxies from Astro-1, these data represent the only FUV spectra of early-type galaxies with wavelength coverage down to the Lyman limit at 912 Å, and thus include the “turnover” in the spectra that is needed to fully characterize the spectral energy distribution. As determined by Burstein et al. (1988) with IUE, the $(m_{1550} - V)$ color varies over a range 2.04–3.86 mag for these galaxies. All of them suffer from a minimal amount of reddening ($0.00 \leq E(B - V) \leq 0.035$ mag).

HUT is uniquely suited for FUV spectroscopy of nearby galaxies. The telescope uses a 90 cm diameter $f/2$ primary mirror and a prime focus, near-normal-incidence, Rowland-circle grating spectrograph to obtain spectrophotometry from 820 to 1840 Å in first order with a resolution of 2–4 Å. The detector consists of a microchannel plate coupled to a phosphor intensifier that is read by a Reticon into 2048 pixels. All six galaxies were observed during orbital night through a $10 \times 56''$ slit. A complete description of the instrument and its calibration is given in Davidsen et al. (1992). Modifications and the resulting performance and calibration for the Astro-2 mission are described in Kruk et al. (1995). The final Astro-1 calibration of HUT is presented in Kruk et al. (1996). The fast focal ratio, large apertures (modified somewhat for Astro-2), and wavelength coverage down to the Lyman limit make HUT an ideal instrument for observing extended objects and for determining the effective temperatures of hot UV sources. For Astro-2, an increase in the effective area by a factor of 2.3, combined with an extended duration flight, allowed HUT to collect much more data with higher signal-to-noise (S/N) than on Astro-1.

Fig. 2 shows the HUT slit superimposed on two different images of the elliptical galaxy M 60 (NGC 4649) and the nearby spiral galaxy NGC 4647. The top panel is an optical image ($\sim 5850\text{--}6820$ Å; Minkowski & Abell 1963) from the Digitized Sky Survey (DSS), and the bottom panel is an FUV image (1344–1698 Å) from the Ultraviolet Imaging Telescope (courtesy of UIT; see also Ohl & O’Connell 1997). The figure demonstrates several important points. Of the six Astro-2 galaxies considered in this paper, M 60 is the only galaxy that has a possible close companion. However, the pairing is likely due to a superposition on the sky: although the two galaxies have similar redshifts, the lack of evidence of tidal interaction, either as tidal plumes or as a distortion of the spiral structure in NGC 4647, suggests that the galaxies are at different distances (Sandage & Bedke 1994). The bottom panel shows that the FUV light is very concentrated in M 60, and that a large percentage of this light falls within the HUT slit. The FUV image also shows that although

the FUV light from the spiral galaxy is more extended than that in the elliptical galaxy, our HUT spectrum is clearly not contaminated by the FUV flux from NGC 4647.

Our six spectra were corrected for airglow contamination from the lines Lyman α λ 1216, Lyman β λ 1026, Lyman γ λ 973, and O I λ 1305 by fitting airglow profiles simultaneously with our model fitting. The spectra were fluxed and corrected for interstellar extinction in our Galaxy using the values of $E(B - V)$ from Table 1, $R_V = 3.05$, and the extinction parameterization of Cardelli, Clayton, & Mathis (1989). For the stellar population model-fitting described in this paper, the HUT data have been binned such that each wavelength point represents 5 HUT bins or 2.5 Å. Only those portions of the observation with stable pointing and the galaxy well centered in the slit were used. Fig. 3 shows the HUT spectra for each of the six Astro-2 galaxies, along with models that will be described below. The NGC 1399 Astro-1 data has been shown in several previous papers (e.g. Ferguson et al. 1991).

3. EVOLUTIONARY MODELS

In order to model the FUV luminosity from the various classes of HB stars and their progeny, we construct synthetic composite spectra for evolved stellar populations by integrating individual synthetic stellar spectra over the stellar evolutionary tracks of DRO93, Bressan et al. (1993), Fagotto et al. (1994a, 1994b, 1994c), and Vassiliadis & Wood (1994). The synthetic stellar spectra come from the grid of Brown et al. (1996) for effective temperature $T_{\text{eff}} \geq 10,000$ K, and from the grid of Kurucz (1992) for $T_{\text{eff}} < 10,000$ K (although these stars below 10,000 K do not significantly contribute to the integrated FUV luminosity). At each point along an evolutionary track, we find the synthetic stellar spectrum closest in T_{eff} and surface gravity (g). To correct for the small mismatch in T_{eff} and g , we scale the bolometric luminosity from the synthetic spectrum so that it matches that in the track step. We then weight the contribution from that point by the time spent at that location in the HR diagram. Our composite spectrum for a given track thus corresponds to a population that enters that track at the rate of one star per year. The normalization of the model and the distance to the galaxy then determine the actual rate of stars entering and leaving the evolutionary tracks, or the stellar evolutionary flux (SEF). Examples of these integrated composite spectra are shown in Fig. 1, for stars evolving along PAGB, PEAGB, and AGBM evolutionary paths.

The diffusion processes in the outer layers of these evolved stars create inconsistencies between the abundances that determine the evolution of the stars and the abundances in the stellar atmospheres of these stars (see §1.2). Because of these inconsistencies, we consider

synthetic spectra with three different atmospheric metallicities ($Z = Z_{\odot}$, $Z = 0.1 Z_{\odot}$, and $Z = 0.01 Z_{\odot}$) for all of the different evolutionary paths, regardless of the inherent abundances driving that evolutionary path. We define Z_{atm} as the abundance of heavy elements driving the *line strengths* in our composite synthetic spectra, and we define Z_{evol} as the abundance of heavy elements driving the *evolution* of stars along the evolutionary path in a given composite synthetic spectrum.

The limitations of our modeling scheme are the following: the small mismatch in temperature and surface gravity between the individual synthetic stellar spectra and the evolutionary track points; the assumption of local thermodynamic equilibrium in the synthetic spectra with $T_{\text{eff}} < 45,000$ K; pure H & He atmospheres for $T_{\text{eff}} \geq 20,000$ K (with metals incorporated only in computing the emitted spectrum, not the atmospheric structures); the lack of continuum opacity for elements heavier than helium for spectra with $T_{\text{eff}} \geq 20,000$ K; and the omission of mass loss during the HB and AGB phases in the DRO93 evolutionary tracks, as well as the usual uncertainties and simplifying assumptions that go into stellar evolution calculations. Errors arising from the tracks are discussed in DRO93 and in §4.3. These limitations may affect the quantitative results, but are less likely to affect the qualitative conclusions.

4. MODEL FITTING

As discussed in the previous section, the normalization of a model fit to the HUT data gives the stellar evolutionary flux (SEF) for stars evolving along the evolutionary path for that model (in the HUT slit). We also have a theoretical value of the SEF_{tot} = the rate of stars evolving along *all* evolutionary paths in the galaxy. For old stellar populations (age $\geq 10^{10}$ yr), the SEF_{tot} per unit luminosity is approximately 2.2×10^{-11} stars L_{\odot}^{-1} yr^{-1} (Greggio & Renzini 1990). There is a dependence of this quantity on composition, particularly on the He abundance, since helium-rich stars at a given mass evolve more quickly. Our models assume that in a galaxy, the dominant population that controls the effective value of the SEF_{tot} has Y close enough to Y_{\odot} such that the solar value of the SEF_{tot} is appropriate. To determine the bolometric luminosity for each of the Astro-2 galaxies, we calculate the V -magnitudes through the HUT slit from archival HST WFPC images, correcting the 0.06 mag color offset between the F555W filter and the Johnson V band and using a bolometric correction (BC) of -1.32 . This BC is consistent with a stellar population of age 12 Gyr and $[\text{Fe}/\text{H}] = 0.25$ (Worthey 1992). For a given evolutionary model fit to the HUT data, normalizing our measured SEF by the bolometric luminosity gives a distance-independent measurement of the fraction of stars evolving along that

evolutionary path, since we know the SEF_{tot} .

For each of the six Astro-2 galaxies, we perform two different classes of fitting: EHB stars alone, or EHB and PAGB stars together. In all of our fitting, we perform χ^2 minimization with the IRAF routine SPECFIT (Kriss 1994). For every model fit to the data, we assume that neutral hydrogen from the interstellar medium (ISM) absorbs at a column depth equivalent to that along a line of sight in our Galaxy, as listed in Table 1.

4.1. EHB tracks

We initially fit EHB composite models based on evolutionary tracks from a variety of groups (DRO93; Bressan et al. 1993; Fagotto et al. 1994a, 1994b, 1994c). While EHB/AGBM sequences from the latter two groups were found to produce reasonable fits to the HUT data, the DRO93 tracks were found to have somewhat superior fits. In addition, they provide a finer mass spacing and the ability to check the effects of Y_{ZAMS} and Z_{evol} separately (as well as the fact that we can compute additional physically consistent sequences where necessary). At fixed chemical composition and envelope mass, spectra constructed with the Fagotto et al. (1994a, 1994b, 1994c) and Bressan et al. (1993) tracks agree with those constructed from the DRO93 tracks. Thus, to simplify the discussion, we limit our analysis to the DRO93 tracks.

The DRO93 tracks are broken into subsets according to the abundances of metals and helium (see their Table 1 and our Table 2); there are eight different abundance combinations. The tracks detail the evolution of HB stars from the zero-age horizontal branch through core He exhaustion, and continue either to the thermally pulsing stage (for AGB evolution) or to the white dwarf cooling track (for AGBM and PEAGB evolution). Each track is parameterized by abundance, ZAHB core mass, and ZAHB envelope mass. We took all 136 tracks in their paper and constructed a corresponding composite spectrum for each track, which was then fit to the HUT data. These spectra were computed with metallicities of $Z_{atm} = Z_{\odot}$, $0.1 Z_{\odot}$, $0.01 Z_{\odot}$. We found that those tracks with $Z_{atm} = 0.1 Z_{\odot}$ best matched the overall absorption features in the HUT data (see §6). The best fit evolutionary model (with $Z_{atm} = 0.1 Z_{\odot}$) for each of the Astro-2 galaxies is listed in Table 3 and plotted in Fig. 3. All of the best fits come from two track sets with high Z_{evol} and Y_{ZAMS} (sets G & H in Table 2). We also include results of the same fitting applied to the spectrum of NGC 1399, which was observed through a $9.4 \times 116''$ slit on Astro-1 (we omit the M 31 Astro-1 data because of the large and uncertain extinction toward that galaxy). The results in Table 3 show that the SEF for EHB stars (SEF_{EHB}) is a small fraction ($\lesssim 10\%$) of the SEF_{tot} . In a model comprised solely of EHB stars, one can reproduce the amount of FUV

light from these galaxies without approaching the limits imposed by the fuel consumption theorem, since EHB stars and their progeny are such efficient FUV emitters. Using the χ^2 statistics to judge the quality of fit, we can compare the quality of the best-fitting EHB model from each abundance group (cf. Table 2) to that of the best fit of any group. We make this comparison in Table 3, which shows a strong preference for groups G and H in the fitting.

We shall use the FUV spectrum of M 60 to demonstrate how models with higher metallicity and helium abundance produce a closer match to the HUT data, since our M 60 spectrum has the best S/N ratio. Fig. 4 shows the best fit $Z_{atm} = 0.1 Z_{\odot}$ model for each of the 8 different abundance (Z_{evol}) sets. In the left column are the evolutionary models for stars with abundances less than or equal to the solar abundance (sets A–D in Table 2). These plots show a significant deficit in the flux at the shortest wavelengths in the model, as compared to the HUT data for M 60. On the other hand, the evolutionary models in the right column, for stars evolving at higher metal and helium abundance (sets E–H in Table 2), show a somewhat smaller flux deficit at the shortest wavelengths. The evolutionary model that fits best is that with $Z_{evol} = 0.04$ and $Y_{ZAMS} = 0.34$ (set G).

If we define the flux deficit as

$$\Delta F = \frac{\sum_{\lambda=912\text{\AA}}^{970\text{\AA}} (F_{data} - F_{model})}{\sum_{\lambda=912\text{\AA}}^{970\text{\AA}} F_{data}}$$

we can characterize the deficit numerically. These deficits (listed in Fig. 4) clearly show that the low Y_{ZAMS} and Z_{evol} models in the left column are more deficient in this wavelength range, as compared to the high Y_{ZAMS} and Z_{evol} models in the right column. However, even the models in the right column show a significant flux deficit. This deficit could be due to the absence of flux from PAGB stars in these models. Because of the high integrated luminosity for stars evolving along EHB tracks (see Fig. 1), the SEF_{EHB} is a small fraction of the rate of all stars evolving along any evolutionary path in these galaxies (the SEF_{tot} ; cf. Table 3). Most of the stars must be evolving along the classical PAGB tracks.

The low-metallicity models appear to have a stronger flux deficit than the high-metallicity models; the reason may be related to the ratio of flux emitted in the HB and post-HB phases. We note that the mean temperature of the integrated spectrum for a given evolutionary sequence depends on the ratio of the radiation emitted in the post-HB

stages to that emitted before core He exhaustion, simply because the mean temperature of AGBM stars is higher than the earlier stage. If one takes the integrated flux below 1200 Å, and computes the ratio of this flux in the post-HB phase to that in the HB phase, one finds that this ratio increases as Y_{ZAMS} and Z_{evol} increases. This is at least a partial explanation why our models tend to favor the higher metallicities.

The models that work best from any of the abundance (Z_{evol} & Y_{ZAMS}) sets and for any Z_{atm} are always those that integrate over AGBM evolutionary tracks (cf. Fig. 1). Models that integrate over PEAGB tracks have spectra that are too cool to agree with the HUT data. We find that a narrow range in envelope mass on the EHB produces spectra that agree reasonably well with the HUT data, consistent with the findings in our previous analysis of these galaxies (Brown et al. 1995). This narrow distribution is on the blue end of the HB with low (but not the lowest) envelope masses on the HB. We discuss the distribution below in the context of the more realistic two-component EHB + PAGB models.

4.2. EHB and PAGB tracks

Because a very small fraction of the stars are evolving along EHB tracks in these galaxies, a more appropriate model to fit to the data is a two-component model, with both EHB stars and PAGB stars. Our PAGB models are constructed by integrating over the six solar-metallicity H-burning tracks of Vassiliadis & Wood (1994) with core masses $M_{core}^{PAGB} = 0.569, 0.597, 0.633, 0.677, 0.754,$ and $0.900 M_{\odot}$. Vassiliadis & Wood (1994) also calculate H-burning tracks at lower metallicities (six at $Z = 0.008$, four at $Z = 0.004$, and two at $Z = 0.001$) and a handful of He-burning tracks. Since all of the H-burning tracks appear qualitatively similar, and since He-burning PAGB evolution is thought to be in the minority ($\lesssim 25\%$; Vassiliadis & Wood 1994 and references therein), we take the six H-burning solar-metallicity tracks as representative of the evolution for classical PAGB stars. We note that all of the Vassiliadis & Wood (1994) tracks start at $T_{\text{eff}} = 10,000$ K in the HR diagram, after the thermally pulsing (TP) stage (see Fig. 1). Our PAGB model spectra thus omit the flux that is generated as the star evolves along the AGB from the HB to the TP stage, since in the HUT wavelength range the contribution from the cool AGB is negligible.

We used two methods to fit two-component (EHB & PAGB) models to the HUT data. The first method allowed the contributions of EHB stars and PAGB stars to float both freely in the fit. The second method constrained the contribution of the PAGB component so that it would not exceed the SEF_{tot} . Assuming that the $\text{SEF}_{\text{tot}} \approx 2.2 \times 10^{-11}$ stars

$L_{\odot}^{-1} \text{ yr}^{-1} \pm 10\%$ (Greggio & Renzini 1990), and that EHB stars by themselves can at most contribute a small fraction ($\lesssim 10\%$) of the SEF_{tot} (from our own fitting in the previous section, and from Brown et al. 1995), we restricted only the PAGB component of the fit, and not the sum of the EHB and PAGB components. Within the uncertainty of the SEF_{tot} , the EHB contribution to the SEF_{tot} is small. This assumption simplifies the χ^2 minimization.

When we did not restrict the PAGB contribution to the model fit, we found that EHB stars from all eight of the DRO93 metallicity groups could reasonably fit the HUT data; the fitting only slightly favored the high Z_{evol} and high Y_{ZAMS} models (sets E–H in Table 2). This was because the short-wavelength deficiencies of the models with $Z_{\text{evol}} < Z_{\odot}$ were compensated by a large PAGB contribution (\approx half of the FUV flux). However, these solutions were not astrophysically consistent, since the PAGB contribution allowed in the fits was much larger than that allowed by the theoretical SEF_{tot} (unless our models severely underestimate the potential UV flux from PAGB stars).

When we restricted the PAGB contribution so that it could not exceed the theoretical SEF_{tot} , we found that the EHB evolutionary models with high Z_{evol} and high Y_{ZAMS} were favored in the fits to the HUT data. The strength of this result is a function of the assumed $M_{\text{core}}^{\text{PAGB}}$ in the galaxies, in the sense that the high Y_{ZAMS} and high Z_{evol} models are more strongly favored as the assumed $M_{\text{core}}^{\text{PAGB}}$ increases. Our results depend upon $M_{\text{core}}^{\text{PAGB}}$ because as the mass increases, the PAGB stars evolve more rapidly and produce less FUV flux over their lifetimes. Thus, if the stellar evolutionary flux of PAGB stars (SEF_{PAGB}) for each $M_{\text{core}}^{\text{PAGB}}$ is limited by the same SEF_{tot} , the more massive PAGB stars will contribute less flux to the EHB + PAGB models than less massive PAGB stars.

Since the strength of our results depends upon the $M_{\text{core}}^{\text{PAGB}}$ assumed, we show these results for the two lowest masses in the set of PAGB models: those with $M_{\text{core}}^{\text{PAGB}} = 0.569 M_{\odot}$ (Table 4 and Fig. 5) and $0.597 M_{\odot}$ (Table 5). Our results are stronger as $M_{\text{core}}^{\text{PAGB}}$ increases, and thus the results in Table 4 represent the conservative results, while those in Table 5 use a $M_{\text{core}}^{\text{PAGB}}$ that is closer to that modelled in the planetary nebula luminosity functions of ellipticals ($0.61 M_{\odot}$; see below). In these EHB + PAGB models, the SEF_{EHB} is a small fraction of the SEF_{tot} predicted by the fuel consumption theorem, while the SEF_{PAGB} is much larger. Note that consistent models only require that $\text{SEF}_{\text{PAGB}} \leq \text{SEF}_{\text{tot}}$, and not $\text{SEF}_{\text{EHB}} + \text{SEF}_{\text{PAGB}} = \text{SEF}_{\text{tot}}$. The value of SEF_{PAGB} that we derive depends on the integrated flux of a particular assumed PAGB track. In reality the PAGB population will have a mass spectrum whose mean mass can be higher and its integrated flux therefore lower, in which case our low-mass PAGB models will underestimate the number of PAGB stars present while overestimating the mean UV contribution from individual stars. The individual PAGB tracks have very similar integrated spectra, and so we cannot constrain

the PAGB mass with our fitting.

Using the χ^2 statistics to judge the quality of fit, we compare in Tables 4 and 5 the quality of the best-fitting EHB + PAGB models from each abundance group (cf. Table 2) to that of the best fit. In Table 4, evolutionary abundances of at least solar are favored in 5 of the 7 galaxies. The exceptions are NGC 3115 and NGC 3379, where there are no preferences for either high or low evolutionary abundances in the fitting. Alternatively, in Table 5, evolutionary abundances greater than the solar value are favored in all 7 of the galaxies, with most fits favoring high Z_{evol} and Y_{evol} . When M_{core}^{PAGB} was increased to even higher values, the fits for all of the galaxies increasingly favored higher Z_{evol} and Y_{ZAMS} . The culmination of this trend was shown in the previous section, where we fit models consisting solely of EHB stars. Such models are equivalent to the assumption that the PAGB stars are too massive to contribute significant flux to the FUV spectra.

What is the appropriate M_{core}^{PAGB} to use in our fitting? Studies of the planetary nebula luminosity function (PNLF) may indicate that $M_{core}^{PAGB} \approx 0.61 M_{\odot}$. The PNLF is well-studied in both spiral bulges and elliptical galaxies. Ciardullo et al. (1989) calibrated the PNLF in the bulge of M 31, and found that it was in excellent agreement with a set of PAGB tracks having a mean M_{core}^{PAGB} of $0.61 M_{\odot}$. Since then, the same PNLF has demonstrated very good agreement with that in the bulge of the Sb galaxy M 81 (Jacoby et al. 1989), in E and S0 galaxies of the Leo I Group (Ciardullo, Jacoby, & Ford et al. 1989), and in E and S0 galaxies of the Virgo Cluster (Jacoby, Ciardullo, & Ford 1990). Four of the Astro-2 galaxies (M 49, M 60, M 87, and NGC 3379) were included in these PNLF studies. In the inner regions (isophotal radius $< 1'$) of the Virgo and Leo I ellipticals, PN were lost in the bright galaxy background, but no significant gradients in the luminosity-specific PN density were seen beyond these regions. Thus, we can not know for certain the characteristics of the PAGB population within the cores of the ellipticals, but the evidence we have points to $M_{core}^{PAGB} \approx 0.61 M_{\odot}$.

In the literature there are other sets of PAGB tracks that extend the range of core masses even lower than the $0.569 M_{\odot}$ track of Vassiliadis & Wood (1994) and thus increase the potential PAGB contribution to the total UV flux. Although it is unlikely that all of the PAGB stars in a galaxy would be evolving along such low-mass tracks (see above), we investigated the effect this would have on our modeling. For example, the Schönberner (1987) set has a track with a core mass of $0.546 M_{\odot}$. Such a low-mass PAGB star evolves so slowly that it contributes significant flux as the PAGB component of an EHB + PAGB model, even when the Schönberner track is restricted by the SEF_{tot} (although we stress that the integrated flux from this $0.546 M_{\odot}$ track does not fit the HUT data by itself, without an EHB/AGBM component). So, EHB + PAGB models that used a $0.546 M_{\odot}$ PAGB

track did not show a preference for either the high Z_{evol} or low Z_{evol} models; the results were similar to those of the unconstrained EHB + PAGB models above. However, Schönberner states that this $0.546 M_{\odot}$ model is below the threshold for the occurrence of thermal pulses; the model is therefore actually a PEAGB sequence. Although pre-TP evolution contributes negligibly to the integrated FUV luminosity of stars evolving along PAGB tracks, the same cannot be said of all PEAGB stars. If we include the luminosity from a $0.550 M_{\odot}$ AGB track (DRO93) as a plausible example of the pre-TP evolution for a star evolving along the $0.546 M_{\odot}$ Schönberner track, we find that the composite spectrum appears similar to the PAGB spectrum in Fig. 1, except that the spectrum rises considerably at wavelengths longer than 1500 \AA , and thus does not agree with the Astro-2 data. The result is that this “PAGB” contribution (which is really PEAGB) in an EHB + PAGB fit to the data is minimized. In summary, the $0.546 M_{\odot}$ track is an acceptable PAGB component only if two conditions are met. First, all of the PAGB stars in the galaxies must evolve along extremely low-mass tracks. Second, the pre-TP evolution must be characterized by high mass stars that are too cool to produce flux in the HUT range while on the AGB, yet lose enough mass on the AGB to subsequently become $0.546 M_{\odot}$ PAGB stars.

Because the “pseudo-continuum” shape is affected by Z_{atm} , the best fitting model was usually, but not always, that with $Z_{atm} = 0.1 Z_{\odot}$. However, at any Z_{atm} , the fitting still favored those evolutionary models with high Z_{evol} and high Y_{ZAMS} . Since the individual absorption features are better matched by $Z_{atm} = 0.1 Z_{\odot}$ (see §6), we chose to demonstrate the best fits to the HUT data by consistently using models with this atmospheric abundance.

Although the models in Fig. 5 fit the Astro-2 data fairly well, there are a few curious discrepancies. The M 49 data shows a large excess at 961 \AA , although the deviation from the model is not very significant. The formal probability of such a deviation from the model flux is 0.16. However, a more significant discrepancy appears in the NGC 3379 data as an emission feature near C IV $\lambda\lambda 1548, 1551$. The feature can be fit by a Gaussian with $\lambda = 1562.7 \text{ \AA}$, equivalent width = 10 \AA , and FWHM = 3000 km s^{-1} . The statistical significance of the feature is 0.0084 (better than a 2σ detection). But what could be causing this feature? We observed NGC 3379 twice, and the same feature shows up in both observations, so it is unlikely that some “glitch” in the data is causing the feature. The deredshifted wavelength of the feature would be 1557.9 \AA , which is still 7 \AA longward of the most likely emission at C IV. If an extraneous emission source fell within the HUT slit, such as a supernova remnant or cooling flow, one would expect to find other emission lines (Ly α , O VI, etc.) at the same redshift. Given the lack of other detectable emission features in the NGC 3379 spectrum, we tentatively conclude the feature is a fluke; a 2σ fluke is not unreasonable given 6 data sets having 410 bins each.

The best-fitting two-component models incorporate EHB tracks with a narrow range in temperature and envelope mass on the EHB, but this range does not include the very lowest envelope masses, which extend down to $0.002 M_{\odot}$. Since the χ^2 contours are probably dominated by the systematic uncertainties of the models, we conservatively use the χ^2 statistics to determine the range of M_{env} that is within 4σ of the best-fit model. We find that in our two-component EHB + PAGB models, a narrow distribution of M_{env} on the EHB fits the Astro-2 data within 4σ , as we found in our initial analysis of these data using lower resolution (10 Å) models (Brown et al. 1995). The range for each galaxy is listed in Tables 4 and 5.

As in the previous section with the one-component (EHB) models, we use the high S/N data for M 60 to demonstrate why models with high Z_{evol} and high Y_{ZAMS} work better than models with low Z_{evol} and low Y_{ZAMS} . Fig. 6 shows the best fit EHB + PAGB model from Table 4, for each of the 8 different abundance (Z_{evol}) sets. In each panel, the PAGB component has $M_{core} = 0.569 M_{\odot}$. The flux deficiency (ΔF) at the shortest wavelengths is more significant in the low Z_{evol} and low Y_{ZAMS} models than in the high Z_{evol} and high Y_{ZAMS} models. However, the high Z_{evol} & Y_{ZAMS} models do still show some deficiency at the shortest wavelengths, and we discuss this problem in the next section.

In our previous study of these galaxies (Brown et al. 1995), we found that PAGB stars alone do not fit the FUV spectral energy distribution of any of the galaxies. This result also holds true in the current study. The result that none of the galaxies can be fit by PAGB stars is significant, because if one were trying to reproduce only the flux at 1550 Å, and not the entire FUV spectral energy distribution observed with HUT, galaxies with very red ($m_{1550} - V$) colors could be accounted for by PAGB stars alone. Hence all of the galaxies in our study appear to require some EHB fraction.

4.3. Systematic Errors

As we discussed above, HB models from DRO93 with supersolar Y_{ZAMS} and Z_{evol} fit the HUT data better than models with subsolar Y_{ZAMS} and Z_{evol} . This is true for both EHB models and EHB + PAGB models. Although the supersolar Y_{ZAMS} and Z_{evol} models work better across the entire HUT range, the largest improvement is in the region shortward of 970 Å. But how much can systematic errors contribute to this result? The major sources of systematic error in our modeling are errors in the individual stellar synthetic spectra, uncertainty in the extinction correction for the galaxies, and uncertainties in the behavior of the input stellar evolution models.

As described in Brown et al. (1996), the Lyman series lines are somewhat too strong in our grid of synthetic stellar spectra. This produces a deficiency in the synthetic spectra as one moves to shorter wavelengths in the HUT range. In Brown et al. (1996), there are six plotted synthetic stellar spectra that have flux down to the Lyman limit, at effective temperatures of 17000 K, 24000 K, 29900 K, 36100 K, 40000 K, and 55000 K, and each has HUT data or a Kurucz LTE model for comparison. If we measure the flux deficiency ΔF for these 6 models, we find that the average deficiency is 0.12 ± 0.08 . Therefore, the supersolar Y_{ZAMS} & Z_{evol} models in the right column of Fig. 6 have deficiencies that fall within the range expected from systematic errors in our individual synthetic spectra, whereas the subsolar Y_{ZAMS} & Z_{evol} models in the left column have deficiencies that fall outside of that range.

The extinction parameterization of Cardelli et al. (1989) does not extend below 1000 Å, but we have extrapolated it to the Lyman limit at 912 Å. Although this results in some uncertainty in the extinction correction, we note that our extinctions are quite low (see Table 1), and thus any errors in the shape of the extinction curve will in turn be quite small. For example, our use of $R_V = 3.05$, characteristic of the very diffuse ISM, produces an extinction correction that deviates from the galactic mean curve ($R_V = 3.1$) by less than 1% when $E(B - V) = 0.035$, which is the highest extinction in Table 1. The significant uncertainty in the extinction is the possibility of extinction intrinsic to the galaxies. However, we note that if the Astro-2 galaxies have internal extinction, our correction for this extinction would increase the flux deficits for all of the models, and thus our supersolar Y_{ZAMS} & Z_{evol} models would still match the Astro-2 data better than those models with subsolar Y_{ZAMS} & Z_{evol} .

The DRO90 tracks neglect the effects of mass loss. If mass loss takes place by winds during the EHB evolution, it is likely to affect the brighter, low-gravity AGBM stage. It will drive the evolution to higher temperatures faster, but since it reduces the available hydrogen fuel it is also likely to reduce the total UV output in these stages. The neglect of mass loss in the tracks should not affect our conclusions regarding metallicity.

4.4. Mass Distribution on the HB

The composite spectrum for a given evolutionary track is the flux one would observe from a population of stars evolving from a single mass on the HB. In reality, the FUV spectra in elliptical galaxies probably arise from populations on the HB (and their progeny) with some distribution of mass. Unfortunately, the true mass distribution on the HB and the mechanisms that govern it remain highly uncertain. These uncertainties are

compounded by the uncertainties in the age and composition of these stellar populations. Thus, there is scant theoretical justification for any given mass distribution.

As an initial attempt to constrain this problem, we tried to fit Gaussian distributions of envelope mass (using a single core mass) to construct our populations, but the best fit always occurred for a δ -function in envelope mass, with the quality of the fits rapidly declining as the width of the Gaussian increased. We believed that a grid of evolutionary tracks with a finer distribution in envelope mass would allow a Gaussian distribution to fit, so we reran the evolutionary code of DRO93 to create a new subset of tracks. These 11 AGBM tracks were evenly spaced by $\Delta M_{env} = 0.002 M_{\odot}$ around the best fit EHB track for M 60 in Table 3 ($M_{env} = 0.036 M_{\odot}$).

We then performed another two-component EHB + PAGB fit to the M 60 HUT data, using the same Z_{atm} and Z_{evol} as the best EHB + PAGB fit in Table 5, but now the EHB contribution came from a Gaussian distribution of envelope mass on the HB, such that the number of stars entering bins of unit envelope mass were constrained by a symmetric Gaussian. We found that a narrow distribution of M_{env} , centered on $M_{env} = 0.042 M_{\odot}$ with FWHM = $0.003 M_{\odot}$, fit the M 60 data slightly better than the original δ -function at $M_{env} = 0.046 M_{\odot}$. While this result suggests that the HB distribution is extremely bimodal, the systematic uncertainties in the model atmospheres and the evolutionary tracks combine to make the constraints weaker than they appear from formal χ^2 fitting. Model spectra constrained with a fairly flat HB distribution are not very different from those with a pure AGBM component, because the long lifetimes make the AGBM stars dominant. For example, increasing the envelope mass FWHM from $0.003 M_{\odot}$ to $0.1 M_{\odot}$ increases χ^2 by 20, and increasing the FWHM to $0.5 M_{\odot}$ increases χ^2 by 32, but the SED in these models still provides a reasonable match to the continuum shape of the HUT data. Thus a “flatter” distribution in *mass* can produce a reasonable SED because the distribution in *flux contribution* is still highly peaked around the AGBM stars. The 4σ limits on the M_{env} distribution given in Tables 5 and 6 denote the limits on which stars can *dominate* the SED.

5. COLOR-COLOR ANALYSIS

The $(m_{1550} - V)$ color of elliptical galaxies is the standard measure of the strength of the UV upturn. If galaxies with stronger UV upturns have a larger fraction of their stellar populations evolving along EHB evolutionary paths than galaxies with weaker UV upturns, it then follows that galaxies with stronger UV upturns should also have a smaller fraction of stars evolving along the classical PAGB tracks (see Brown et al. 1995 and Ferguson & Davidsen 1993). While the $(m_{1550} - V)$ color tracks the strength of the FUV flux relative to

the optical flux, the $(m_{<1000} - m_{1550})$ color tracks the “characteristic” temperature of the FUV population. Using the HUT data and archival HST images, we define these colors as

$$(m_{<1000} - m_{1550}) = 2.5 \log_{10} \frac{\langle f_{\lambda=1450-1650\text{\AA}} \rangle}{\langle f_{\lambda=912-1000\text{\AA}} \rangle}$$

and

$$(m_{1550} - V) = 2.5 \log_{10} \frac{f_{V_o}}{\langle f_{\lambda=1450-1650\text{\AA}} \rangle}$$

where $\log f_{V_o=10} = -12.41 \text{ ergs cm}^{-2} \text{ s}^{-1} \text{ \AA}^{-1}$ (Johnson 1966), and V_o is derived from the V and $E(B - V)$ values in Table 1.

The left-hand panel of Fig. 7 shows the color-color diagram for the six Astro-2 galaxies and for NGC 1399 (we again omit the Astro-1 galaxy M 31 because of the large and uncertain extinction toward that galaxy). The dashed line shows the shift in $(m_{1550} - V)$ that would occur if we used the measurements of Burstein et al. (1988) through the smaller IUE apertures. The large extent and variation in the dashed lines is a clear indication of the strong variation in the FUV/optical flux ratio as a function of radius in these galaxies. These differences in color gradients are apparent in the simultaneous UIT observations of these galaxies (O’Connell et al. 1992; Ohl & O’Connell 1997).

In the right-hand panel, we show the variation in $(m_{<1000} - m_{1550})$ for the integrated spectra of models in abundance group G (Table 2). The four reddest of these models (DRO93) stop at the TP stage (and produce negligible FUV flux), so we have tacked on plausible PAGB evolution from Vassiliadis & Wood (1994). The $(m_{<1000} - m_{1550})$ color appears “hot” for the high and low extremes of HB mass (respectively HB/PAGB and EHB/AGBM). As one moves from the blue end of the HB to larger envelope masses, the flux from the EHB stars and their progeny becomes progressively “cooler” in the FUV. This trend may explain the positions of the HUT data points in the left-hand panel. The hot NGC 1399 spectrum may be dominated by stars evolving from the blue extreme of the HB, while the hot FUV spectra of M 49, NGC 3115, and NGC 3379 may have significant contribution from PAGB stars. The “cooler” FUV spectra of M 60 and M 89 may be dominated by AGBM stars with higher envelope masses than those in NGC 1399. Of course, with only a handful of galaxies, it is premature to deduce a correlation between the behavior seen in the data and that shown in the right-hand panel of Fig. 7. But this type of color-color diagram might be a useful tool in future studies.

M 87, which has an active nucleus, might have other reasons for its position in the color-color diagram. The active galaxies in the Burstein et al. (1988) study did not follow

the UV-Mg₂ relation of the quiescent galaxies. However, recent HST observations have shown that the FUV flux from the point source and jet in the M 87 nucleus cannot be contributing significantly to the HUT spectrum (Tsvetanov et al. 1996). Also, subtracting the nuclear flux from the V measurement through the HUT slit would only diminish V and make the ($m_{1550} - V$) color even bluer. So why is M 87 so blue in both of the colors in Fig. 7? We believe that the answer may be related to the position of M 87 in the Virgo cluster. Because M 87 lies at the center of this cluster, it has been accreting gas and metals from other galaxies. Perhaps this accretion has altered the stellar evolution in M 87 so that it is markedly different from that in the other Astro-2 galaxies. For example, a recent episode of star formation could dramatically decrease ($m_{<1000} - m_{1550}$) but not affect ($m_{1550} - V$) significantly. If we start with the best fit EHB + PAGB model for M 60, and add a third component representing continuous star formation (SF) for the past 10^7 yr at the rate of $0.16 M_{\odot} \text{ yr}^{-1}$ with a normal (Salpeter) IMF, we find that we can reproduce the M 87 HUT flux. Although the total accretion rate from the M 87 cooling flow is estimated at $20\text{--}30 M_{\odot} \text{ yr}^{-1}$ (White & Sarazin 1988), the rate of star formation is generally a small fraction of the cooling rate in giant ellipticals; the fraction has been calculated as high as 15 % in some cases, but $\lesssim 1$ % in many others (O’Connell & McNamara 1988). In our EHB + PAGB + SF model, $\text{SEF}_{\text{EHB}} = 2.8 \times 10^{-2} \text{ stars yr}^{-1}$ and $\text{SEF}_{\text{PAGB}} = 0.36 \text{ stars yr}^{-1}$. If we compare these numbers to those in Tables 4 and 5, we see that adding the young stars means the ratio of EHB to PAGB stars in M 87 would be more in line with the ratio in M 60. Although this small number of young stars would make ($m_{<1000} - m_{1550}$) significantly bluer, their contribution to the V band would be negligible, since this flux is dominated by a much larger number of RGB stars. Unfortunately, the S/N in the M 87 data is low enough that we cannot put limits on the contribution of young stars using the C IV and Si IV absorption. In contrast, the NGC 1399 data is of higher S/N, and the lack of detectable C IV and Si IV absorption in the NGC 1399 spectrum makes star formation an unlikely explanation for its FUV colors (cf. Ferguson et al. 1991).

6. LINE STRENGTHS

Although the line strengths in our FUV spectra probably do not reflect the inherent abundances driving the evolution in these galaxies, they can still tell us information about the abundances in the atmospheres of stars in these evolved populations. We found that EHB + PAGB models with $Z_{\text{atm}} = 0.1 Z_{\odot}$ best reproduced the overall absorption features in the HUT data. Fig. 8 shows the M 60 data and the best fit EHB + PAGB model for M 60 (Table 4), but with three different atmospheric metallicities: $Z_{\text{atm}} = Z_{\odot}$, $0.1 Z_{\odot}$, and $0.01 Z_{\odot}$. It is obvious that the practically featureless $0.01 Z_{\odot}$ model (bottom panel)

has absorption lines that are too weak to match the HUT data. In contrast, the Z_{\odot} model (top panel) has absorption lines which are mostly too strong. Most of the absorption lines are best matched in the $0.1 Z_{\odot}$ model (center panel), although the broad blanketing from Fe absorption at 1550 Å and 1000 Å might be better matched in the Z_{\odot} model. Thus, in M 60, the atmospheric metal abundance is likely to be somewhere in the range $0.1\text{--}1 Z_{\odot}$.

To quantify the atmospheric abundances in these populations and to look for any correlation between the line strengths and colors, we measure the absorption line strengths empirically, by absorption line fitting and spectral indices. These two methods do not rely upon stellar evolutionary models or synthetic spectra. However, in practice, the low S/N in the HUT data hampers these measurements and makes it difficult to draw strong conclusions regarding the atmospheric abundances in these populations.

6.1. Spectral Indices

By using the EHB models as a guide, we can define spectral indices which reflect the abundances of elements responsible for strong absorption features in the FUV: C, N, Si, and Fe. While C, N, and Si each have a small number of strong features in the HUT wavelength range, Fe produces strong line blanketing over large regions of this range (Brown et al. 1996).

We define line and continuum regions for C, N, Si, and Fe, and then measure the spectral index I in magnitudes as

$$I = 2.5 \log_{10} \frac{N_{cont}^{-1} \sum_{cont} F_{\lambda}}{N_{lines}^{-1} \sum_{lines} F_{\lambda}},$$

where N_{cont} and N_{lines} are the number of continuum bins and line bins, respectively.

Table 6 lists the line and continuum regions used to define our spectral indices. Because the FUV is completely blanketed by absorption lines, there is no way to define a “clean” spectral index that will be affected by absorption from only a single element (see Figs. 9–12 in Brown et al. 1996). To show how these indices may change as a function of abundance in a stellar atmosphere, we measured the indices in an LTE synthetic stellar spectrum with $T_{\text{eff}} = 25,000$ K, $\log g = 5.0$, and $Z_{atm} = Z_{\odot}$. We repeated this measurement in synthetic spectra where one of four elements (C, N, Si, and Fe) was missing, and the results are plotted in Fig. 9. Because the indices are not completely “clean,” the index from one element can be affected by the abundance of other elements (see for example the effect of

removing Fe in the upper right panel of Fig. 9). However, it is apparent in the figure that these indices are sensitive to the individual abundance changes in these four elements.

To improve the S/N, we combined the deredshifted spectra from galaxies with strong UV upturns (M 60 and M 89) to produce a “UV-strong” spectrum, and the deredshifted spectra from galaxies with weak UV upturns (M 49, NGC 3115, and NGC 3379) to produce a “UV-weak” spectrum. The individual spectra were weighted by the variance in this process. We then measured the spectral indices in both the UV-strong and UV-weak spectra. The UV-strong and UV-weak spectra are plotted in Fig. 10, along with the regions used for the spectral index measurements.

Fig. 11 shows the variation in these indices vs. Z_{atm} , for each of the EHB + PAGB models shown in Fig. 6 and Table 4. In this way, we can account for the spread in indices due to the uncertainties in Z_{evol} : each panel shows the indices as a function of Z_{atm} for a model from each of the Z_{evol} groups in Table 2. On the left-hand side of each panel, we plot the indices for the UV-weak and UV-strong Astro-2 data. These indices are shown as error bars that encompass the 1σ statistical uncertainties. Because these uncertainties are fairly large, we cannot use the indices to determine accurately what the atmospheric abundances are in the stellar populations in these galaxies. However, it is evident in Fig. 11 that the indices are consistent with $Z_{atm} \approx 0.1 Z_{\odot}$. It is also apparent that the HUT data exhibit a weak trend, such that the UV-strong galaxies tend to have stronger UV spectral indices than the UV-weak galaxies; seven of the nine indices in Fig. 11 show this tendency.

6.2. Absorption Line Fitting

We attempted to fit absorption lines in the two Astro-2 galaxies with reasonable S/N: M 60 and NGC 3379. Each of these galaxies was observed multiple times during the Astro-2 mission, in order to improve the S/N in two galaxies with very different UV upturn strengths. We also fit these same features in the best-fit EHB + PAGB model for M 60 ($Z_{atm} = 0.1 Z_{\odot}$; Table 4). The fits to the two galaxies and the model are listed in Table 7.

The low S/N of the Astro-2 data required that we restrict the number of free parameters in our absorption line fits. Thus, we fit Gaussian absorption profiles to those features listed in Table 7, holding the FWHM and the line center fixed. The FWHM was held to the quadrature sum of the intrinsic line width (determined from the EHB + PAGB model), the velocity dispersion in the nucleus of each galaxy, and the 3 \AA resolution of the HUT data. The velocity dispersions of M 60 and NGC 3379 are 363 and 214 km s^{-1} respectively (Burstein et al. 1988). The uncertainties in equivalent width (EW) are calculated from

the 1σ errors, the upper limits in EW are calculated for the 2σ confidence level, and the significance is the formal probability that the absorption feature results from a statistical fluctuation.

An analysis of the line strengths in Table 7 does not provide any indication of systematic changes between the absorption lines in the UV-strong M 60 and those in the UV-weak NGC 3379. However, given the statistical uncertainty in these measurements, a correlation between the FUV colors and the FUV absorption line strengths could easily be lost in the noise. The absorption lines are again consistent with $Z_{atm} \approx 0.1 Z_{\odot}$.

7. DISCUSSION AND SUMMARY

Each individual analytical technique we have employed provides evidence for somewhat weak conclusions about the chemical composition of the stellar populations in these galaxies. Taken in their entirety, our results favor the hypothesis that the FUV light from elliptical galaxies originates in a population with high metallicity and possibly high He abundance. These conclusions appear to depend on the ratio of post-HB to EHB flux derived from the tracks. The results for the tracks with $Z_{evol} > Z_{\odot}$ are less distinguished from each other than they are from those of lower metallicity in this respect, so that more specific conclusions cannot be drawn. We cannot, however, from the FUV spectra alone, rule out the low-metallicity scenario of Park & Lee (1997).

The preceding sections have demonstrated:

- 1) The HUT Astro-1 and Astro-2 E galaxy spectra are best fit by a composite EHB + PAGB star model; the FUV spectra are dominated by EHB stars following AGBM evolution.
- 2) When the flux from the PAGB component is constrained by the fuel consumption theorem, EHB stars of high Y_{ZAMS} and Z_{evol} are favored to make up the flux deficit near the Lyman limit.
- 3) Absorption features are consistent with $Z_{atm} \simeq 0.1 Z_{\odot}$ and may tend to increase as the UV upturn increases, but the direct constraints on metallicity from spectral lines are weak due to the low S/N of the data and the likely redistribution of elements within the EHB star atmospheres.

If EHB stars alone could account for the FUV light in elliptical galaxies, then EHB stars with high Z_{evol} and high Y_{ZAMS} would best fit the Astro-2 data. However, we know that PAGB stars exist in ellipticals; we can observe bright PAGB stars in elliptical galaxies, and the fuel consumption theorem tells us that the stars evolving from the EHB are only a small fraction of the entire evolved population. If all of the stars in the population

evolved from the EHB, the FUV light from ellipticals would be much brighter than that observed, since EHB stars are such efficient FUV emitters. Dorman et al. (1995) estimate $(m_{1550} - V) \sim 0$ for systems where all of the HB stars lose sufficient mass on the RGB to become EHB and subsequently AGBM stars (i.e. sdB and then sdO stars). Hence the theoretical bluest possible $(m_{1550} - V)$ color implies ~ 6 times more FUV radiation than is observed in the nucleus of bluest galaxy, NGC 1399. Since we know PAGB stars make up the bulk of the FUV population and contribute to at least a fraction of the FUV light, a more realistic approach is a two-component EHB + PAGB model. If the EHB and PAGB components are fit to the HUT data without fuel consumption constraints, then the HUT data can be reproduced equally well by populations with low Z_{evol} & Y_{ZAMS} or high Z_{evol} & Y_{ZAMS} . The ambiguity occurs because a “hot” PAGB spectrum can offset the flux deficit at short wavelengths in the low Z_{evol} and Y_{ZAMS} models. However, an unconstrained EHB + PAGB model is unrealistic, because in such fits the number of PAGB stars exceeds that allowed by the fuel consumption theorem. Although the EHB and unconstrained EHB + PAGB models are instructive, a more realistic model is one where the number of PAGB stars is astrophysically plausible and thus constrained by the fuel consumption theorem. When we fit these constrained EHB + PAGB models to the HUT data, the fitting favors a population evolving with high Z_{evol} and high Y_{ZAMS} .

The EHB stars that best fit the Astro-1 and Astro-2 data in any EHB or EHB + PAGB model are those that lie within a narrow distribution of envelope mass on the low-mass (blue) end of the HB. The stars in this narrow distribution evolve along AGBM paths, but the mass distribution does not include those EHB stars with the very lowest envelope masses on the HB. In addition, since the SEDs of PEAGB stars are so dissimilar to the Astro-2 data (see Fig. 1), PEAGB stars cannot comprise a significant fraction of the stellar populations in these galaxies. This result is partly to be expected from the small mass range that produces them for a given Y and Z . However, it is possible (and plausible) that relatively low mass PEAGB stars (with $\log L/L_{\odot} \sim 3.2$) are produced in old populations through mass loss on the AGB. Such objects are in principle capable of supplying the total UV flux for the weaker UV upturn systems (with $m_{1500} - V \gtrsim 3.6$). Our modeling implies that all of the galaxies we have studied instead have some significant contribution from a small EHB population. From this we infer that the galaxies have a bimodal HB population in general. Nesci & Perola (1985) showed that a strongly bimodal temperature distribution on the HB was needed to explain the 2200 Å dip seen in IUE spectra of elliptical galaxies, and Ferguson (1994) invoked a bimodal temperature distribution to explain the SEDs of the Astro-1 observations of NGC 1399 and M 31, since a uniform distribution of mass on the HB would produce a “flatter” spectrum (Ferguson 1994) than observed.

The open cluster NGC 6791 might be an analog of the situation in elliptical galaxies,

since it shows a high-metallicity evolved population with a strongly bimodal temperature and mass distribution on the HB (Liebert et al. 1994). However, the existence of this cluster might present problems to the theorists in both the high-metallicity and low-metallicity camps in the elliptical galaxy composition debate. It is also possible that this cluster *may not* be providing us direct information about mass loss in the single stars of metal rich systems, since several of the observed stars are binaries (E. M. Green 1996, private communication) which may have affected the evolution of the giant before core helium ignition, by tidal interaction and by mass ejection. However, bimodality occurs in globular cluster HB morphology as well (e.g. NGC 1851; Walker 1992), where binarism is much less common. We currently lack the understanding to explain the existence of a bimodal mass distribution in a coeval, single-metallicity population. The mass-loss mechanisms on the RGB that determine the distribution of mass on the HB are the largest source of uncertainty in the evolution of these populations.

Given a bimodal HB distribution where the efficient UV emitters are on the EHB, the $(m_{1550} - V)$ color should track that fraction of stars evolving from the EHB, while the $(m_{<1000} - m_{1550})$ color should track the “characteristic” temperature of the FUV population. The uncertainties in mass distribution on the HB means that we will need more than seven data points to understand the behavior in a color-color diagram like that shown in Fig. 7. However, these FUV colors are consistent with the scenario proposed by Ferguson & Davidsen (1993) that UV-weak galaxies have a relatively large PAGB contribution to their spectra, while the UV-strong galaxies are dominated by EHB stars and their AGBM progeny, evolving from a range of temperatures on the blue end of the HB. In the future, with more data points in such a color-color diagram, we might be able to deduce information about the HB mass distribution.

Park & Lee (1997) argue that stars in the low-metallicity tail of an extended metallicity distribution are responsible for the UV upturn seen in elliptical galaxies. Bressan et al. (1994) believe that a high-metallicity population produces the UV flux in these galaxies, and they explore metallicities as high as $Z = 0.05$. If the absorption features in evolved populations reflect their intrinsic abundances, then the actual situation in elliptical galaxies lies somewhere in between these two extremes, since the absorption features in the HUT data are consistent with $Z_{atm} \simeq 0.1 Z_{\odot}$. There is a weak trend in the spectra of these galaxies, such that galaxies with stronger UV upturns show stronger UV line indices. This trend is in the opposite sense to that predicted by Park & Lee (1997), but in agreement with the predictions of Bressan et al. (1994) and Dorman et al. (1995).

However, diffusion processes in the envelopes of stars in evolved populations tend to enhance low intrinsic abundances and diminish high intrinsic abundances, and thus it is

unlikely that $Z_{atm} = Z_{evol}$. Given this situation, we must also compare the spectral energy distributions predicted by modeling the FUV data. This comparison supports the theory that the strength of the UV upturn in elliptical galaxies is directly tied to that fraction of a high Z_{evol} and high Y_{ZAMS} population evolving along AGBM tracks from the blue end of the horizontal branch. Integrations over high Z_{evol} and high Y_{ZAMS} evolutionary tracks best fit the HUT data, and AGBM evolution is more easily produced in a high Z_{evol} and high Y_{ZAMS} population, providing a natural explanation for the correlation between UV upturn strength and metallicity found by Burstein et al. (1988).

Of course, the large uncertainties in our analysis mean that we cannot rule out the Park & Lee (1997) hypothesis. The χ^2 statistics in our fitting favor the high Y & Z_{evol} models, but to the eye one can produce reasonable matches to the HUT data with integrations over low Y & Z_{evol} tracks. In the Park & Lee work, they argue that the FUV flux is dominated by a population with $[Fe/H] < -0.7$, but unfortunately it is difficult to discern from their paper the exact distributions in M_{env} and metallicity which are used in their models. Furthermore, although Park & Lee stress that their purpose is not to match the actual SEDs observed in ellipticals, it seems that their synthetic spectra are too flat in the FUV, at least in comparison to the overplotted IUE data (cf. their Figs. 6 & 10). It would be interesting to apply their models to the HUT data, in order to determine if their low metallicity models can reproduce the actual SEDs of observed ellipticals, including the flux near the Lyman limit, since our analysis indicates that the low Y & Z tracks do not reproduce the short wavelength flux needed to reproduce the HUT SEDs.

In order to answer definitively the debate and disentangle the effects of age and metallicity on the HB mass distribution, data with higher S/N for a larger sample of galaxies is required. At higher S/N, it should be obvious if diffusion processes are playing a large role in the strengths of the FUV absorption lines, since observations of evolved stars show lines that deviate strongly from solar abundances or even scaled solar abundances. However, we should not restrict our study to the strengths of metallic lines. The hydrogen lines are also very sensitive to the effective temperature and surface gravity of the different HB evolutionary phases. Inspection of Fig. 1 shows that PAGB spectra have a much shallower Lyman series than that seen in AGBM spectra. Although the S/N in the HUT data was not sufficient to use the Lyman series as a stellar population probe, accurate measurements of the flux below Lyman α (and thus beyond the detection capabilities of HST) will yield important information about the relative numbers of PAGB and AGBM stars in a given population. Such observations could be made with another flight of HUT or a similar successor. Fortunately, future FUV measurements of elliptical galaxies will be accompanied by the rapid progress currently seen in the calculation of synthetic stellar spectra. The near future should bring the emergence of fully line-blanketed, non-LTE model

atmospheres and synthetic spectra, and with these models, another source of uncertainty will be removed from our understanding of the FUV data.

Once we know the chemical composition of the FUV sources in elliptical galaxies, the resolution of the debate will have impact beyond the study of stellar evolution. Elliptical galaxies show great promise as standard candles and tracers of cosmic evolution. The understanding of the FUV flux from galaxies will also enable us to decode the information stored in the longer UV wavelengths (Dorman & O’Connell 1996). The different composition hypotheses each argue for different ages of the Universe and different scenarios for the construction of the galaxies. Under the Park & Lee (1997) low-metallicity scenario, the more massive galaxies formed first, in contrast to the “bottom-up” cosmologies wherein the giant elliptical galaxies formed from the merger of smaller galaxies. In this way, the metallicity debate has consequences that extend to important issues in cosmology and galaxy evolution.

This work was supported by NASA contract NAS 5-27000 to the Johns Hopkins University. B. D. acknowledges partial support from NASA RTOP 188-41-51-03. We wish to thank Jeffrey Kruk and Gerard Kriss for their assistance with the reduction of the HUT data. We also wish to thank T. Stecher and the UIT team for providing the FUV image of M 60, and R. Ciardullo for useful discussion.

The optical M 60 DSS image is based on photographic data of the National Geographic Society – Palomar Observatory Sky Survey (NGS-POSS) obtained using the Oschin Telescope on Palomar Mountain. The NGS-POSS was funded by a grant from the National Geographic Society to the California Institute of Technology. The plates were processed into the present compressed digital form with their permission. The DSS was produced at the Space Telescope Science Institute under US Government grant NAGW-2166.

REFERENCES

- Bergeron, P., Wesemael, F., Michaud, G., & Fontaine, G. 1988, *ApJ*, 332, 964
- Bressan, A., Chiosi, C., & Fagotto, F. 1994, *ApJS*, 94, 63
- Bressan, A., Fagotto, F., Bertelli, G., & Chiosi, C. 1993, *A&AS*, 100, 647
- Brocato, E., Matteucci, F., Mazzitelli, I., & Tornambè, A. 1990, *ApJ*, 349, 458
- Burstein, D., & Heiles, C. 1984, *ApJS*, 54, 33
- Burstein, D., Bertola, F., Buson, L. M., Faber, S. M., & Lauer, T. R. 1988, *ApJ*, 328, 400
- Brown, T. M., Ferguson, H. C., & Davidsen, A. F. 1995, *ApJ*, 454, L15
- Brown, T. M., Ferguson, H. C., & Davidsen, A. F. 1996, *ApJ*, 472, 327
- Cardelli, J. A., Clayton, G. C., & Mathis, J. S. 1989, *ApJ*, 345, 245
- Ciardullo, R., Jacoby, G. H., Ford, H. C., & Neill, J. D. 1989, *ApJ*, 339, 53
- Ciardullo, R., Jacoby, G. H., & Ford, H. C. 1989, *ApJ*, 344, 715
- Davidsen, A. F., et al. 1992, *ApJ*, 392, 264
- Dorman, B. 1992, *ApJS*, 80, 701
- Dorman, B. & O’Connell, R. W. 1996, in *From Stars to Galaxies: The Impact of Stellar Physics on Galaxy Evolution*, eds. C. Leitherer, U. Fritze von Alvensleben, & J. P. Huchra, (San Francisco: ASP), 105
- Dorman, B., O’Connell, R. W., & Rood, R. T. 1995, *ApJ*, 442, 105
- Dorman, B., Rood, R. T., & O’Connell, R. W. 1993, *ApJ*, 419, 596 (DRO93)
- Fagotto, F., Bressan, A., Bertelli, G., & Chiosi, C. 1994a, *A&AS*, 104, 365
- Fagotto, F., Bressan, A., Bertelli, G., & Chiosi, C. 1994b, *A&AS*, 105, 29
- Fagotto, F., Bressan, A., Bertelli, G., & Chiosi, C. 1994c, *A&AS*, 105, 39
- Ferguson, H. C. 1995, in *IAU Symp. 164, Stellar Populations*, ed. P. Van der Kruit (Dordrecht: Reidel), 239
- Ferguson, H. C. et al. 1991, *ApJ*, 382, L69
- Ferguson, H. C., & Davidsen, A. F. 1993, *ApJ*, 408, 92
- Ferguson, H. C., & Sandage, A. 1990, *AJ*, 100, 1
- Gregg, M. D. 1994, *AJ*, 108, 2164
- Greggio, L., & Renzini, A. 1990, *ApJ*, 364, 35.
- Hanes, D. A., & Harris, W. E. 1986, *ApJ*, 304, 599

- Horch, E., Demarque, P., & Pinsonneault, M. 1992, *ApJ*, 388, L53
- Jacoby, G. H., Ciardullo, R., Ford, H. C., & Booth, J. 1989, *ApJ*, 344, 704
- Jacoby, G. H., Ciardullo, R., & Ford, H. C. 1990, *ApJ*, 356, 332
- Johnson, H. R. 1966, *ARAA*, 4, 191
- Kaler, J. B., & Jacoby, G. H. 1991, *ApJ*, 382, 134
- Kriss, G. A. 1994, in *ASP Conference Proceedings 61, Astronomical Data Analysis Software and Systems III*, ed. D. R. Crabtree, R. J. Hanisch, & J. Barnes (San Francisco: ASP), 437
- Kruk, J. W. et al. 1995, *ApJ*, 454, L1.
- Kruk, J. W. et al. 1996, *ApJ*, submitted.
- Kurucz, R. L. 1992, in *IAU Symposium 149, The Stellar Populations of Galaxies*, ed. B. Barbuy & A. Renzini (Dordrecht: Kluwer Press), 225
- Lamontagne, R., Wesemael, F., & Fontaine, G. 1987, *ApJ*, 318, 844
- Lee, Y.-W. 1994, *ApJ*, 430, L113
- Lee, Y.-W., Demarque, P., & Zinn, R. 1994, *ApJ*, 423, 248
- Liebert, J., Saffer, R. A., & Green, E. M. 1994, *AJ*, 107, 1408
- Michaud, G., Vauclair, G., & Vauclair, S. 1983, *ApJ*, 267, 256
- Minkowski, R. L., & Abell, G. O. 1963, in *Basic Astronomical Data*, ed. K. Aa. Strand (Chicago: University Chicago Press), 481
- Minniti, D., 1995, *A&A*, 300, 109
- O’Connell, R. W. et al. 1992, *ApJ*, 395, L45
- O’Connell, R. W., & McNamara, B. R. 1988, in *Cooling Flows in Clusters and Galaxies*, ed. A. C. Fabian (Dordrecht: Reidel), 103
- Ohl, R., & O’Connell, R. W. 1997, *ApJ*, in prep.
- Park, J.-H., & Lee, Y.-W. 1997, 476, in press
- Reimers, D. 1975, *Mém. Soc. Roy. Sci. Liège*, 6^e Ser., 8, 369
- Saffer, R. A., & Liebert, J. 1995, in *Proceedings of the 9th European Workshop on White Dwarfs*, eds. D. Koester & K. Werner (Berlin: Springer), 221
- Sandage, A., & Bedke, J. 1994, in *The Carnegie Atlas of Galaxies, Volume 1* (Washington D.C.: Carnegie Institute of Washington), 51

- Schönberner, D. 1987, in IAU Symposium 131, Planetary Nebulae, ed. S. Torres-Peimbert (Dordrecht: Kluwer Academic Publishers), 463
- Sarajedini, A., Lee, Y.-W., & Lee, D.-H. 1995, ApJ, 450, 712
- Sweigart, A. V. & Gross, P. 1976, ApJS, 32, 367
- Tsvetanov, Z. et al. 1997, ApJ, in prep.
- Vassiliadis, E., & Wood, P. R. 1994, ApJS, 92, 125
- Walker, A. R. 1992, PASP, 104, 1063
- White III, R. E., & Sarazin, C. L. 1988, 335, 688
- Worthey, G. 1992, Ph.D. thesis, Univ. California, Santa Cruz
- Yi, S., Afshari, E., Demarque, P., & Oemler, Jr., A. 1995, ApJ, 453, L69

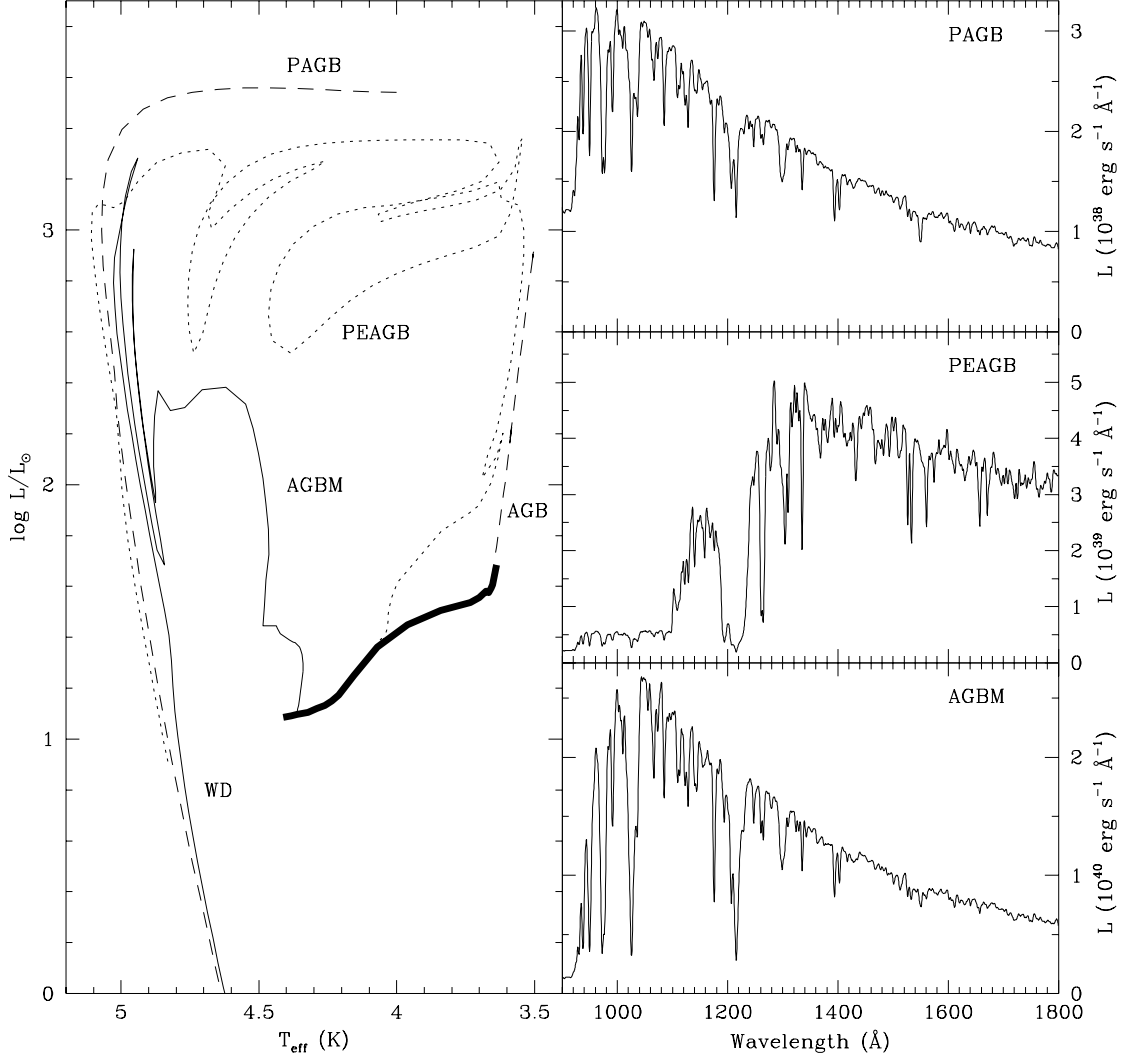


Fig. 1.— The three classes of evolution for stars on the HB produce very different FUV spectra when one integrates the FUV luminosity over these tracks, assuming that stars enter each track at the rate of one star per year. The gap between the AGB evolution ($M_{env} = 0.231 M_{\odot}$; dashed; DRO93) and the PAGB evolution ($M_{core} = 0.569 M_{\odot}$; dashed; Vassiliadis & Wood 1994) is due to the uncertainties in the TP phase. All of the evolutionary paths assume solar abundances, and the luminosities are integrated over the synthetic spectra grids of Brown, Ferguson, & Davidsen (1996) and Kurucz (1992), again assuming solar abundances. Note that the integrated luminosity from the AGBM track ($M_{env} = 0.006 M_{\odot}$; thin solid; DRO93) is much higher than that from the PEAGB track ($M_{env} = 0.051 M_{\odot}$; dotted; DRO93), which in turn is higher than that from the PAGB track (dashed). The heavy solid line denotes the ZAHB.

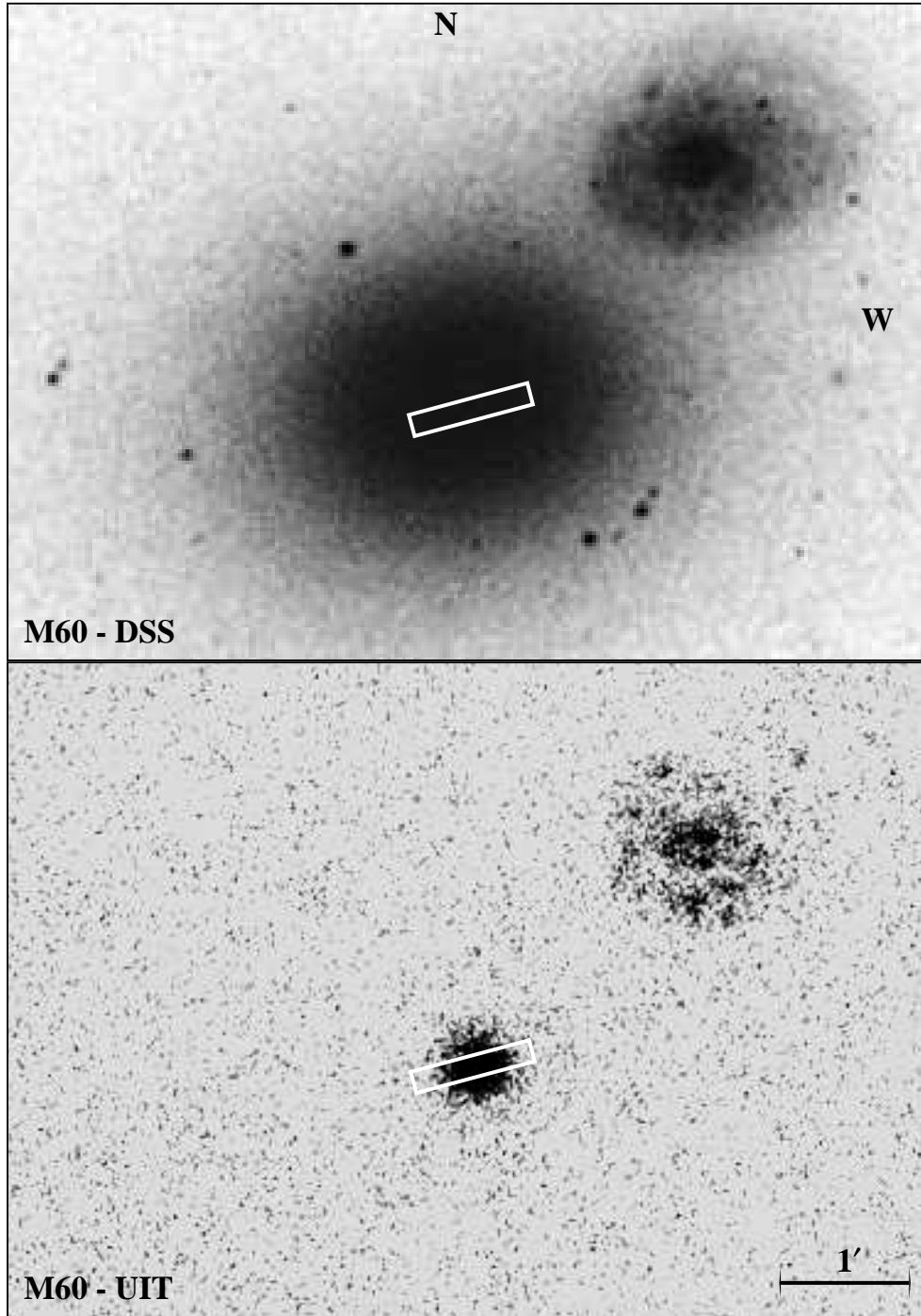


Fig. 2.— The optical image (top panel) and the FUV image (bottom panel) of M 60 and NGC 4647 demonstrate that there is no evidence for tidal interaction between the two galaxies, that much of the concentrated FUV light from M 60 fell within the HUT slit (white rectangle), and that light from NGC 4647 is unlikely to contaminate the HUT data for M 60.

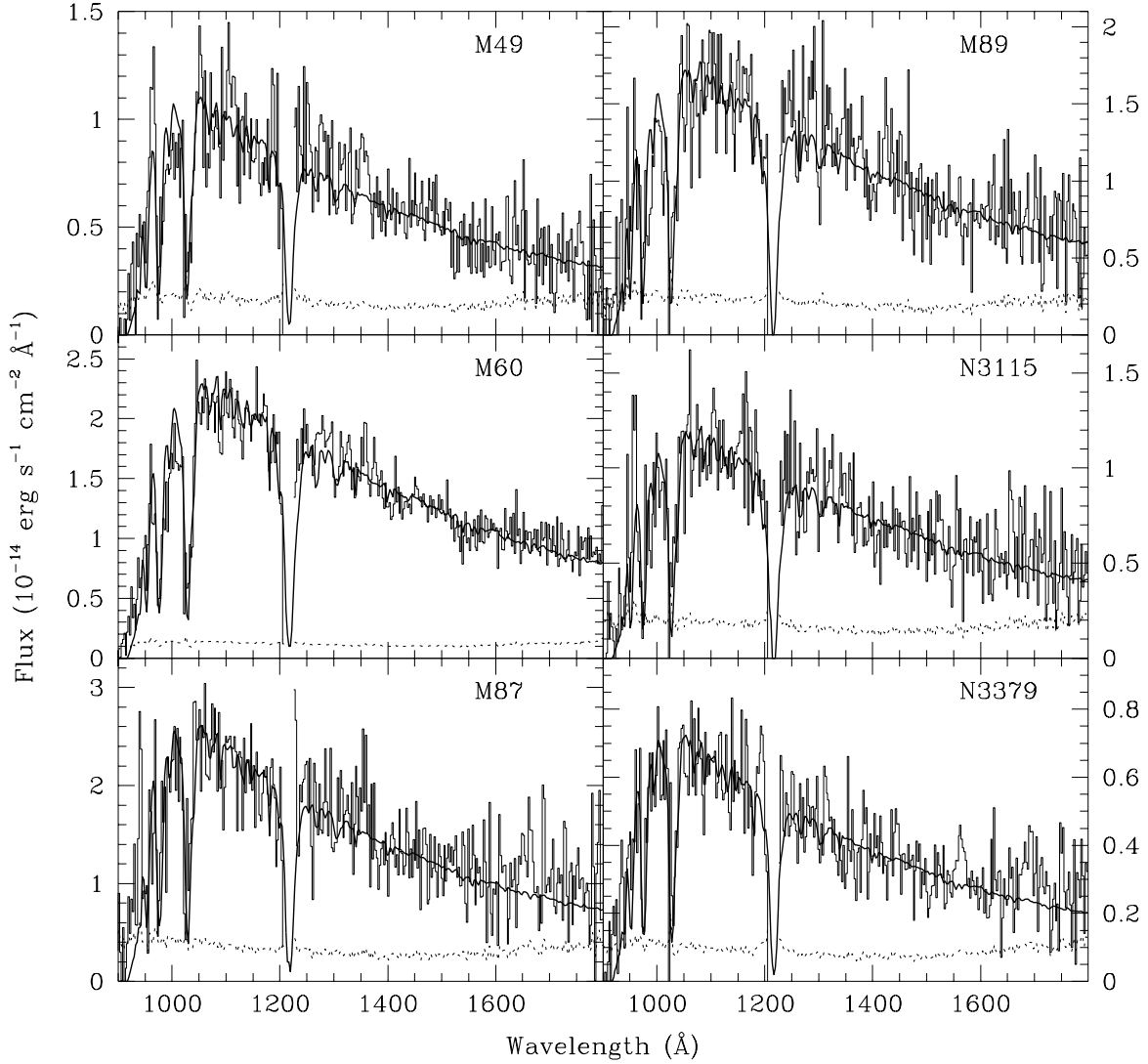


Fig. 3.— Fig. 3— The best fit evolutionary model (solid) from integrations over EHB tracks is plotted over the HUT data (solid; histogram; binned by 2.5 \AA) for each of the Astro-2 observations. The evolutionary models integrate over synthetic spectra with $Z_{atm} = 0.1 Z_{\odot}$, which best reproduces the absorption features in the Astro-2 data, especially in the higher S/N data of M 60. Statistical errors in the data are shown dotted.

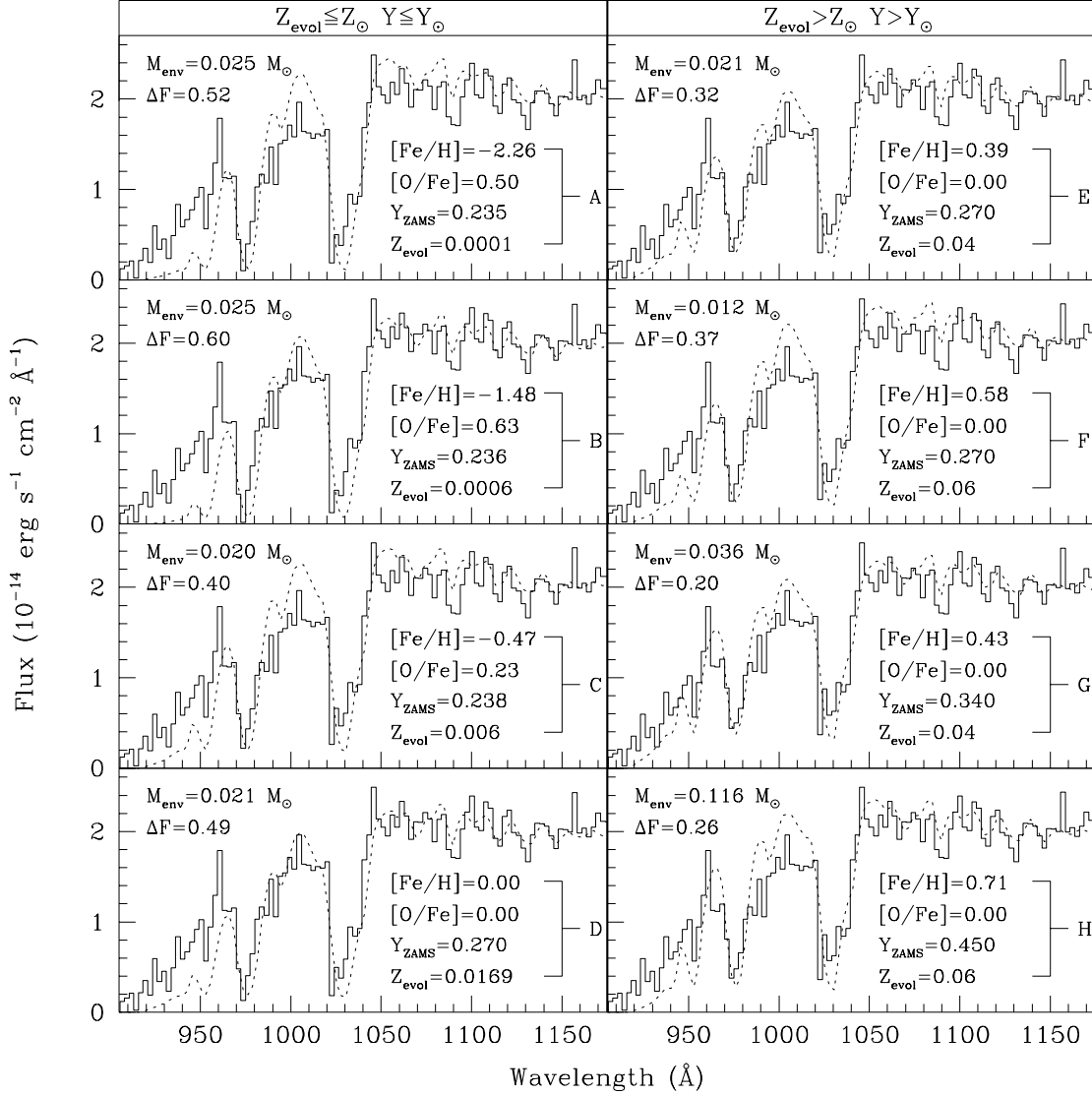


Fig. 4.— The best fit evolutionary model (dashed) from each of the DRO93 abundance subsets (Table 2) shows that EHB stars with high Z_{evol} and high Y_{ZAMS} fit the M 60 data (solid histogram) better than the EHB stars with low Z_{evol} and low Y_{ZAMS} . The abundances and envelope mass driving the evolution for each of the evolutionary tracks is given in each panel, and $Z_{atm} = 0.1 Z_{\odot}$. Part of the reason the models with supersolar evolutionary abundances (right column) fit better than those with subsolar abundances (left column) is the flux deficiency shortward of 970 Å (ΔF).

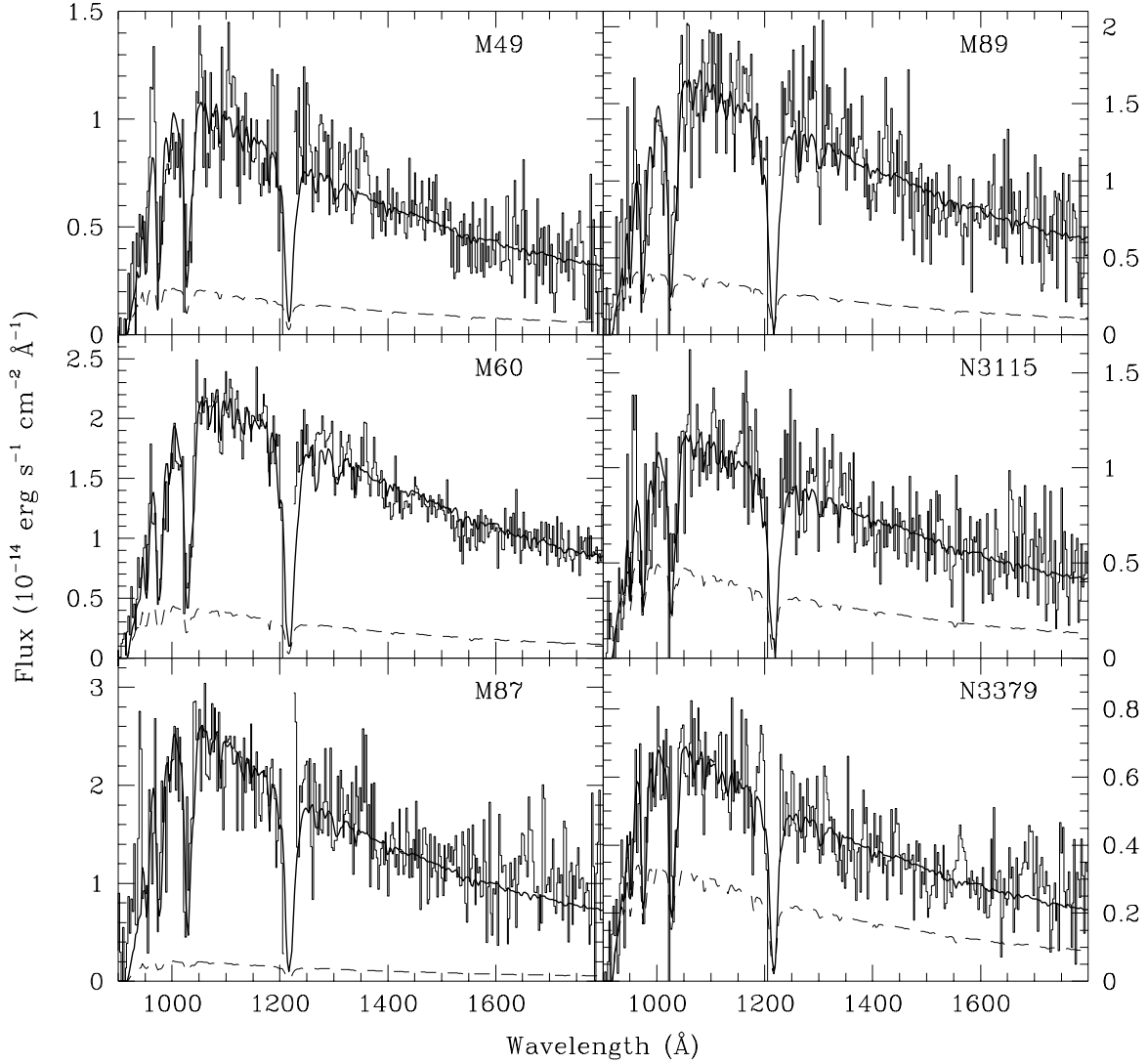


Fig. 5.— The best fit evolutionary model (solid) from two-component models integrating over EHB and PAGB tracks is plotted over the HUT data (solid histogram; binned by 2.5 \AA) for each of the Astro-2 observations. As in Fig. 3, the evolutionary models have $Z_{atm} = 0.1 Z_{\odot}$. Instead of statistical errors, the PAGB contribution to each two-component model is shown dashed.

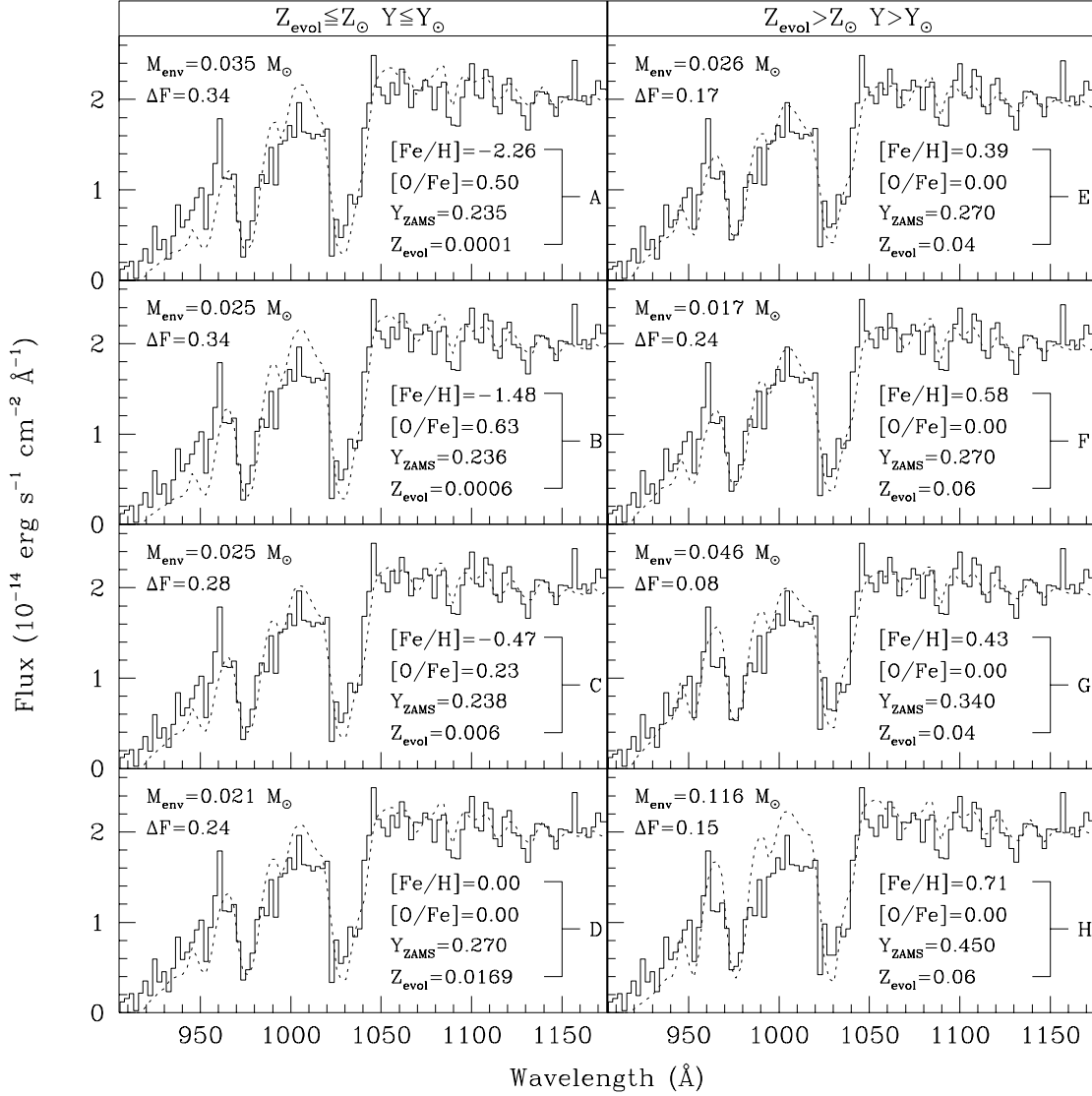


Fig. 6.— The same as in Fig. 4, except that the model (dashed) now has two components: EHB stars and PAGB stars. The PAGB component comes from the $Z_{\text{evol}} = Z_{\odot}$ set of Vassiliadis and Wood (1994), with $M_{\text{core}} = 0.569 M_{\odot}$. The legend on each of the eight plots reflects the abundances which drive the evolution of the DRO93 EHB tracks. The models with subsolar evolutionary abundances (left column) again show significant flux deficiencies shortward of 970 \AA (ΔF).

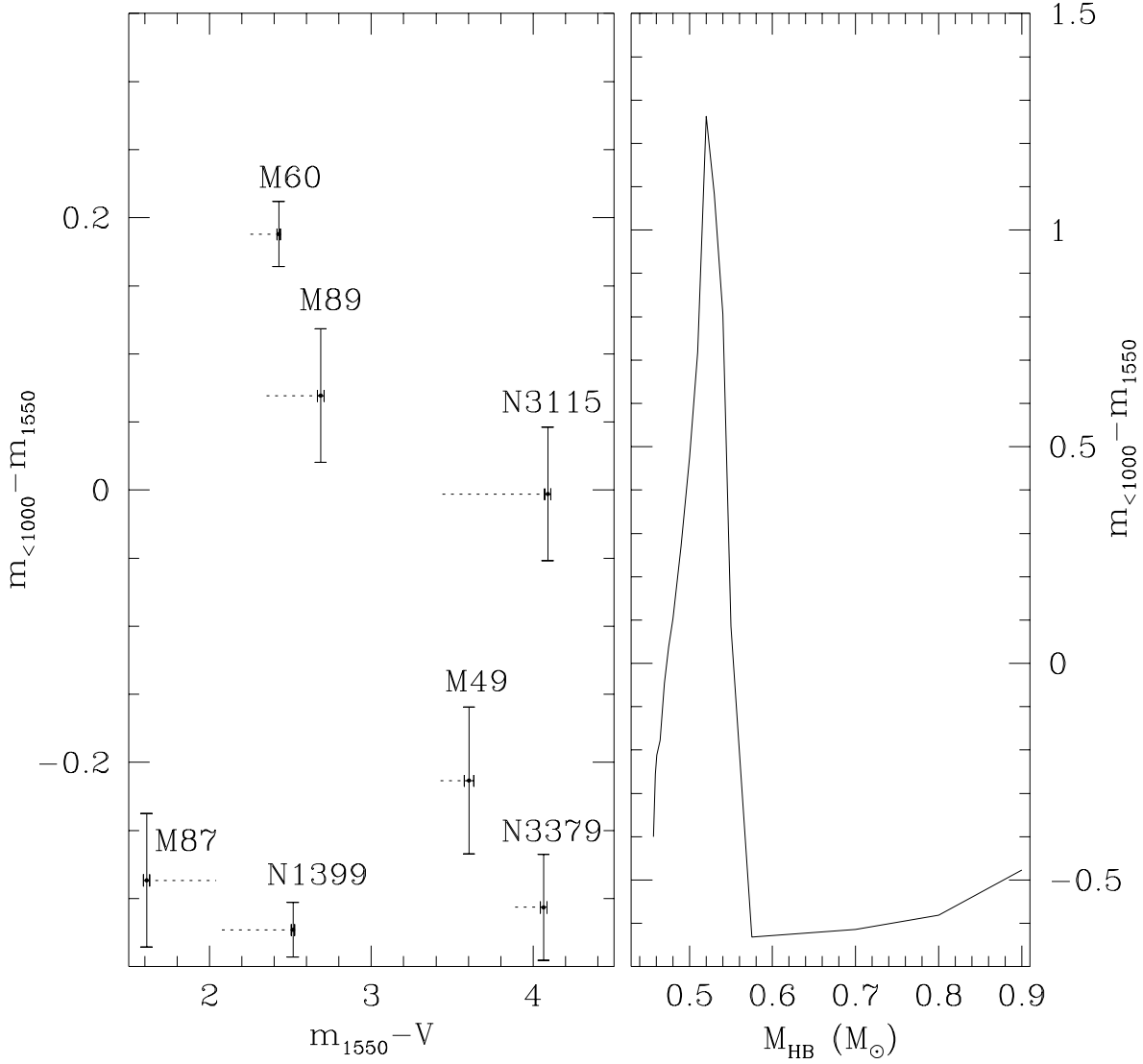


Fig. 7.— The $(m_{<1000} - m_{1550})$ colors in the integrated synthetic spectra change considerably as a function of envelope mass on the HB (right panel). PAGB stars evolving from the red end of the HB and EHB stars evolving from the extreme blue end of the HB both show hotter $(m_{<1000} - m_{1550})$ colors, while stars evolving between these extremes appear cooler. Thus, in the color-color diagram (left panel), galaxies with strong UV-upturns (NGC 1399, M 60, M 89) may be dominated by EHB stars evolving from narrow ranges of envelope mass on the blue end of the HB, while galaxies with weaker UV-upturns (M 49, NGC 3115, NGC 3379) may have significant FUV contributions from PAGB stars. Error bars show the 1σ statistical uncertainty, and the dashed lines show the shift in $(m_{1550} - V)$ color that would occur if we used the Burstein et al. (1988) measurements.

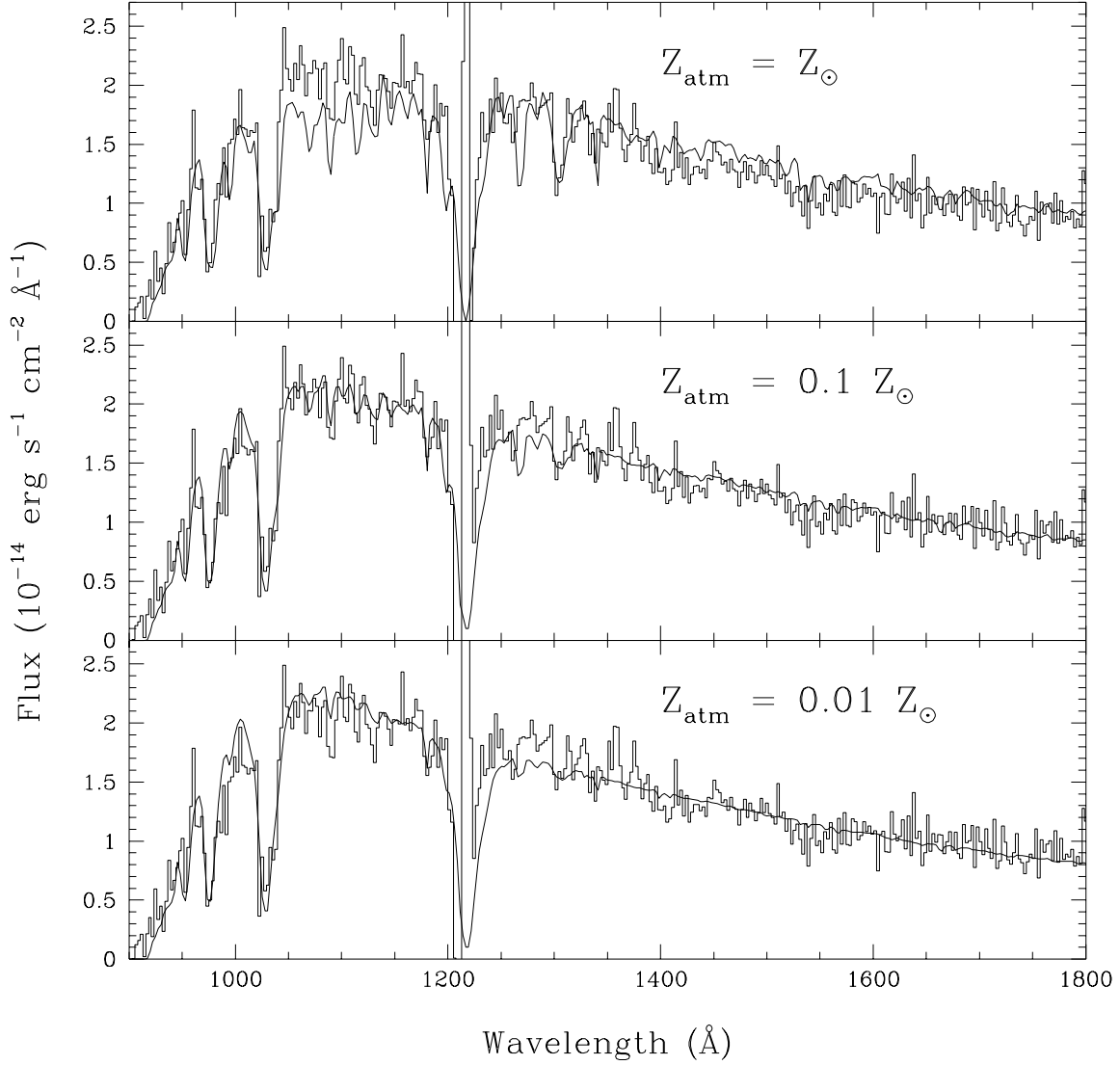


Fig. 8.— The HUT data for M 60 (histogram) are plotted with the best fit EHB + PAGB model (solid) for M 60, given in Table 3. The EHB + PAGB model integrates over synthetic spectra with $Z_{atm} = Z_{\odot}$, $0.1 Z_{\odot}$, and $0.01 Z_{\odot}$. The absorption features fit best in the center panel, with $Z_{atm} = 0.1 Z_{\odot}$. Small differences in the data shown in each panel are due to variations in the airglow subtraction, since airglow profiles were fit simultaneously with the models.

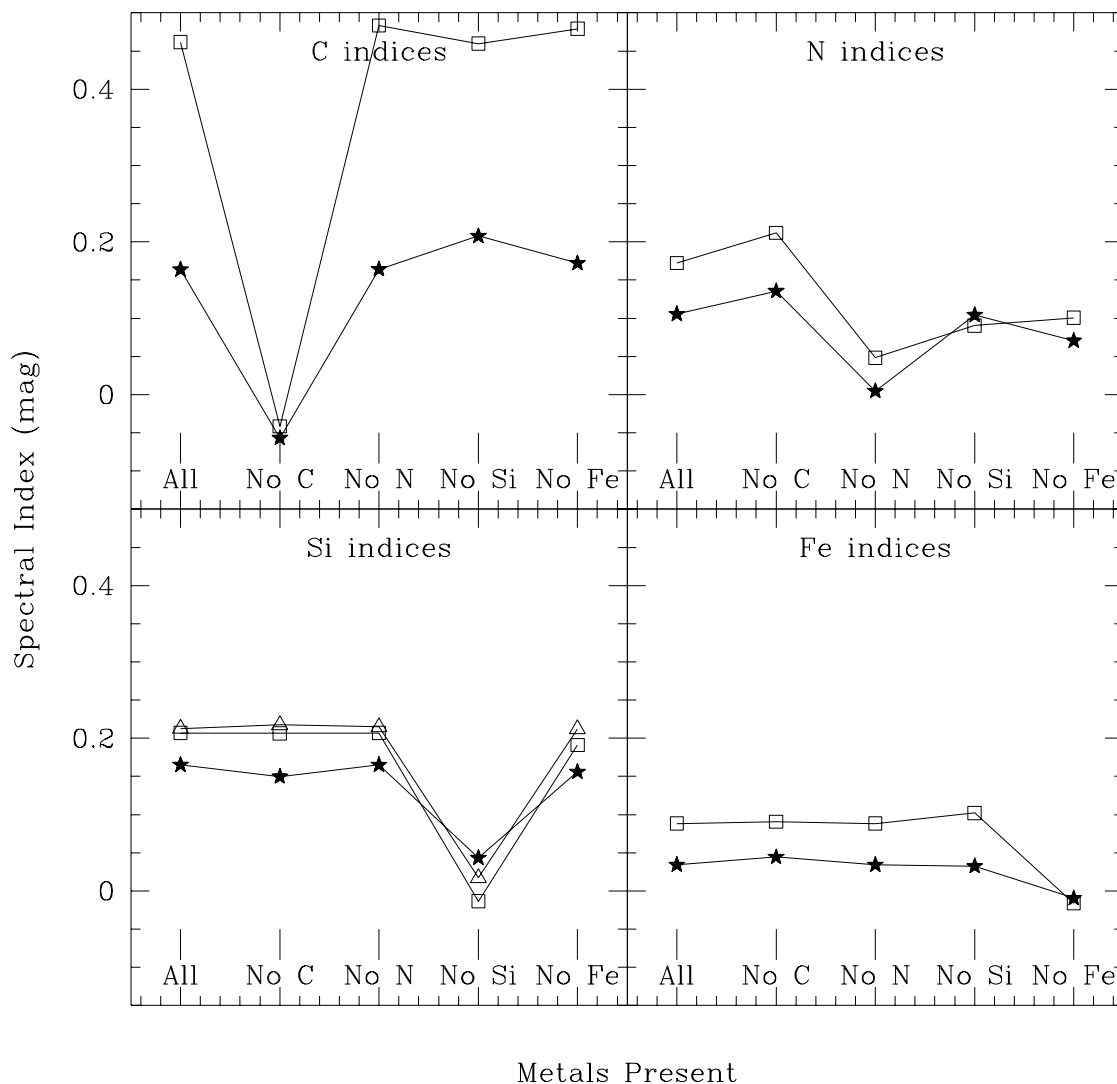


Fig. 9.— The spectral indices for synthetic spectra with $T_{\text{eff}} = 25,000$ K and $\log g = 5.0$ are plotted for spectra at solar abundance (labeled All) or at solar abundance with one element missing (labeled). The line blanketing in the FUV prevents the definition of a “clean” spectral index that is affected by only one element, but these indices show the most sensitivity to the intended elements. The indices are defined in Table 2.

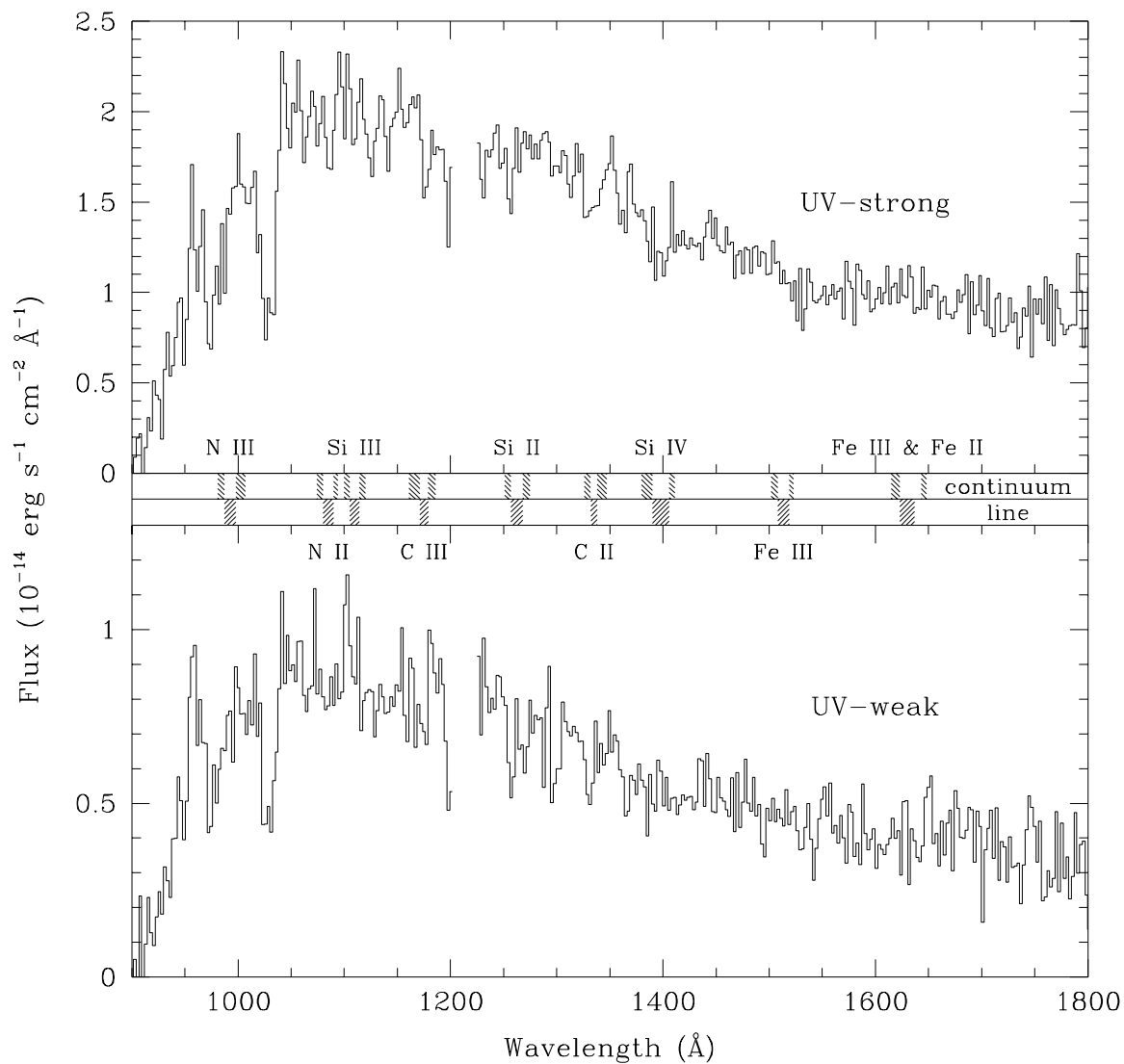


Fig. 10.— The “UV-strong” spectrum (top panel) is the variance-weighted average of M 60 and M 89, and the “UV-weak” spectrum (bottom panel) is the variance-weighted average of M 49, NGC 3115, and NGC 3379. The line and continuum regions used in the spectral index measurements are indicated.

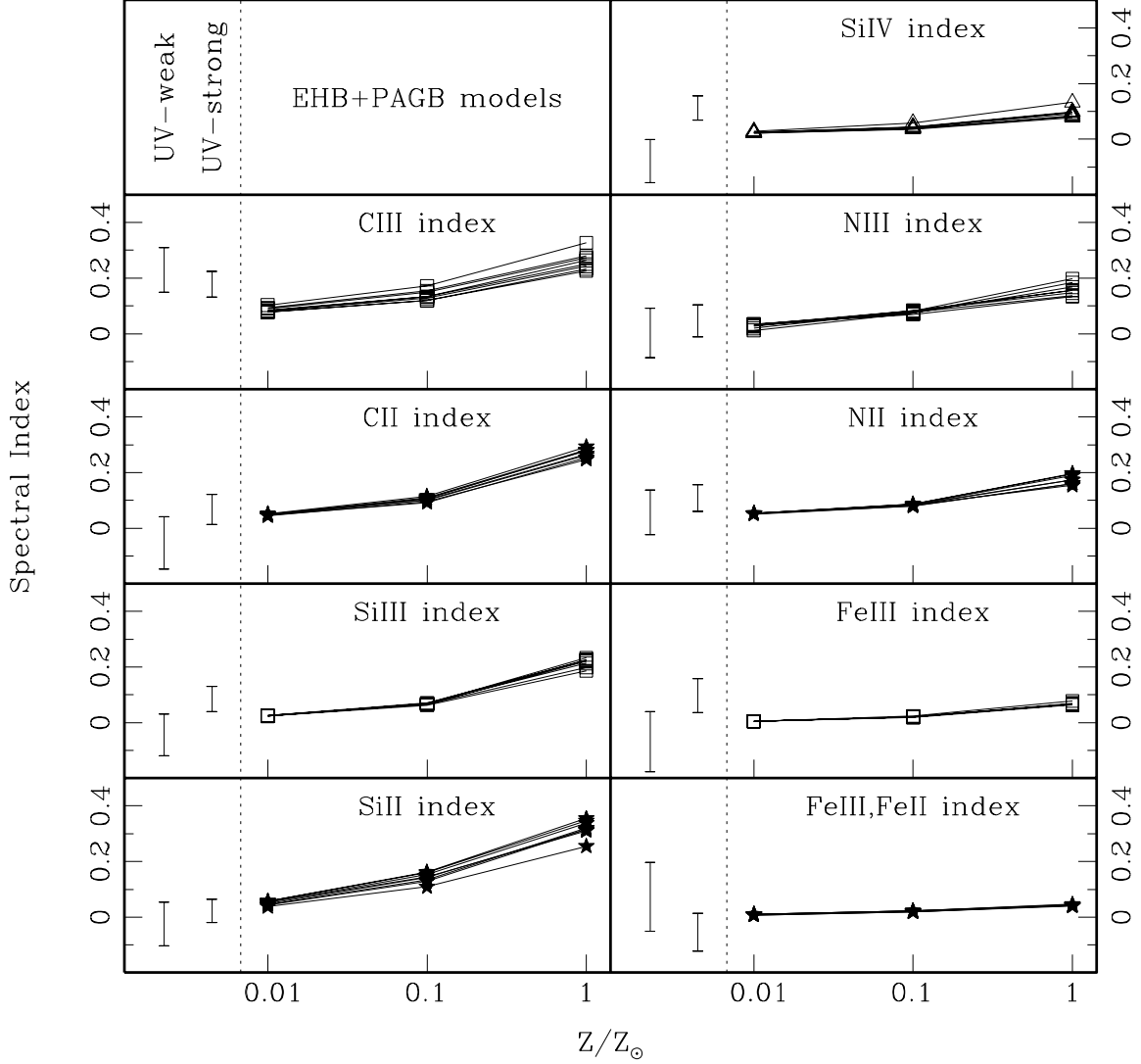


Fig. 11.— The spectral indices from Table 4, plotted for EHB+PAGB models and the Astro-2 data. The UV-weak galaxies (M 49, NGC 3115, and NGC 3379) were averaged to form a composite UV-weak spectrum, and the UV-strong galaxies (M 60 and M 89) were averaged to form a composite UV-strong spectrum. In order to account for spectral index variations due to evolutionary assumptions, we have plotted in each panel a given spectral index vs. Z_{atm} for eight EHB+PAGB models (one from each of the eight Z_{evol} subsets in Table 2). Specifically, each EHB+PAGB model is taken from the best-fit models to M 60 that are shown in Fig. 6. Note that the data are consistent with low atmospheric abundances (Z_{atm}), with the UV-strong galaxies tending toward stronger indices.

Table 1: HUT Astro-2 Observations

	M 49	M 60	M 87	M 89	NGC 3115	NGC 3379
Exp. (sec)	1346	5224	950	1682	1634	3074
D (Mpc)	21.9 ^a	21.9 ^a	21.9 ^a	21.9 ^a	10.0 ^b	18.2 ^a
V (mag) ^c	11.19	11.46	12.30	11.60	10.54	11.24
H I (10^{20} cm ²) ^d	1.64	2.41	2.51	2.50	4.44	2.86
$E(B - V)$ (mag) ^e	0.000	0.010	0.023	0.035	0.025	0.013
$(m_{1550} - V)$ (mag) ^f	3.60 ± 0.03	2.43 ± 0.01	1.61 ± 0.02	2.69 ± 0.02	4.09 ± 0.02	4.07 ± 0.02
$(m_{<1000} - m_{1550})$ (mag) ^g	-0.21 ± 0.05	0.19 ± 0.02	-0.29 ± 0.05	0.07 ± 0.05	-0.00 ± 0.05	-0.31 ± 0.04

^aFerguson & Sandage 1990

^bHanes & Harris 1986

^cThrough the HUT slit, from archival HST data.

^dEinstein On-Line Service, Smithsonian Astrophysical Observatory

^eBurstein & Heiles 1984

^fThrough the HUT slit, from HUT and archival HST data.

^gThrough the HUT slit.

Table 2: Evolutionary Models

Set	[Fe/H]	[O/Fe]	Z_{evol}	Y_{ZAMS}	Y_{HB}	M_{core}
A	-2.26	0.50	0.0001	0.235	0.245	0.495
B	-1.48	0.63	0.0006	0.236	0.247	0.485
C	-0.47	0.23	0.0060	0.238	0.257	0.475
D	0.00	0.00	0.0169	0.270	0.288	0.469
E	0.39	0.00	0.0400	0.270	0.292	0.464
F	0.58	0.00	0.0600	0.270	0.289	0.458
G	0.43	0.00	0.0400	0.340	0.356	0.454
H	0.71	0.00	0.0600	0.450	0.459	0.434

Table 3: Stellar Population Modelling– EHB Fitting

	M 49	M 60	M 87	M 89	NGC 3115	NGC 3379	NGC 1399
SEF _{tot} (stars yr ⁻¹) ^a	0.94	0.76	0.36	0.72	0.39	0.65	0.84
Best Z_{evol} group	H	G	H	G	G	H	H
M_{env} (M_{\odot})	0.086	0.036	0.076	0.036	0.036	0.076	0.016
χ^2/ν	1.2	2.9	1.7	1.7	1.3	1.3	3.0
SEF _{EHB} (stars yr ⁻¹) ^b	2.1×10^{-2}	5.7×10^{-2}	5.1×10^{-2}	4.3×10^{-2}	6.2×10^{-3}	9.7×10^{-3}	8.1×10^{-2}
$\Delta\chi^2$ for alternative abundance groups ^c							
A	39	371	64	47	43	47	211
B	30	370	51	50	40	37	142
C	20	218	40	25	26	35	97
D	21	181	40	27	29	35	81
E	17	34	34	3	9	31	71
F	24	176	6	18	21	18	65
G	4	0	11	0	0	15	40
H	0	88	0	13	10	0	0

^aThrough the HUT slit, based on the fuel consumption theorem and V -magnitude from Table 1.

^bThrough the HUT slit, based upon fitting the HUT FUV data.

^cBy statistical comparison to the best-fit EHB model for each galaxy. ν is 272 for NGC 1399, and 326 for the Astro-2 galaxies.

Table 4: Stellar Population Modelling– EHB + PAGB Fitting ($M_{core}^{PAGB} = 0.569 M_{\odot}$)

	M 49	M 60	M 87	M 89	NGC 3115	NGC 3379	NGC 1399
SEF _{tot} (stars yr ⁻¹) ^a	0.94	0.76	0.36	0.72	0.39	0.65	0.84
Best Z_{evol} group	G&H	E	H	D&F	B&F	C&H	H
M_{env} (M_{\odot})	0.026	0.026	0.056	0.017	0.017	0.116	0.016
χ^2/ν	1.2	2.6	1.6	1.7	1.3	1.2	3.0
M_{env} 4 σ limits ^b	0.007–0.116	0.021–0.046	0.016–0.106	0.012–0.046	0.012–0.166	0.007–0.166	0.011–0.026
SEF _{EHB} (stars yr ⁻¹) ^c	2.1×10^{-2}	5.6×10^{-2}	3.9×10^{-2}	4.1×10^{-2}	4.7×10^{-3}	4.8×10^{-3}	6.8×10^{-2}
SEF _{PAGB} (stars yr ⁻¹) ^c	0.38	0.76	0.36	0.72	0.18	0.41	0.84
$\Delta\chi^2$ for alternative abundance groups ^d							
A	5	131	47	13	3	1	211
B	3	118	43	15	0	1	142
C	1	37	30	4	2	0	97
D	2	16	32	0	3	1	81
E	2	0	24	2	2	3	71
F	2	21	7	0	0	2	65
G	0	3	6	8	5	4	40
H	0	144	0	27	7	0	0

^aThrough the HUT slit, based on the fuel consumption theorem and V -magnitude from Table 1.

^bIn any Z_{evol} group.

^cThrough the HUT slit, based upon fitting the HUT FUV data.

^dBy statistical comparison to the best-fit EHB+PAGB model for each galaxy. ν is 271 for NGC 1399, and 325 for the Astro-2 galaxies.

Table 5: Stellar Population Modelling– EHB + PAGB Fitting ($M_{core}^{PAGB} = 0.597 M_{\odot}$)

	M 49	M 60	M 87	M 89	NGC 3115	NGC 3379	NGC 1399
SEF _{tot} (stars yr ⁻¹) ^a	0.94	0.76	0.36	0.72	0.39	0.65	0.84
Best Z_{evol} group	G	G	H	E	F	H	H
M_{env} (M_{\odot})	0.026	0.046	0.056	0.021	0.017	0.076	0.021
χ^2/ν	1.2	2.7	1.6	1.7	1.3	1.2	3.0
M_{env} 4σ limits ^b	0.011–0.106	0.046–0.046	0.016–0.106	0.012–0.116	0.017–0.166	0.011–0.86	0.011–0.026
SEF _{EHB} (stars yr ⁻¹) ^c	2.1×10^{-2}	5.3×10^{-2}	5.1×10^{-2}	4.1×10^{-2}	4.9×10^{-3}	7.5×10^{-3}	9.7×10^{-2}
SEF _{PAGB} (stars yr ⁻¹) ^c	0.018	0.76	0.36	0.71	0.33	0.38	0.84
$\Delta\chi^2$ for alternative abundance groups ^d							
A	30	233	55	22	7	20	211
B	26	217	47	23	5	17	142
C	10	130	35	13	3	5	97
D	15	72	36	3	4	40	81
E	3	39	28	0	1	12	71
F	20	107	4	9	0	24	65
G	0	0	8	3	3	1	40
H	3	123	0	16	5	0	0

^aThrough the HUT slit, based on the fuel consumption theorem and V -magnitude from Table 1.

^bIn any Z_{evol} group.

^cThrough the HUT slit, based upon fitting the HUT FUV data.

^dBy statistical comparison to the best-fit EHB+PAGB model for each galaxy. ν is 271 for NGC 1399, and 325 for the Astro-2 galaxies.

Table 6: Spectral Indices

Ion	Line region (\AA)	Continuum regions (\AA)	Plot symbol ^a
C III	1171–1179	1161–1171, 1179–1186	□
C II	1332–1338	1326–1332, 1338–1347	★
N III	987–998	981–987, 998–1007	□
N II	1080–1090	1074–1080, 1090–1094	★
Si III	1105–1114	1100–1105, 1114–1120	□
Si II	1257–1268	1251–1257, 1268–1275	★
Si IV	1390–1406	1380–1390, 1406–1411	△
Fe III	1508–1519	1502–1508, 1519–1523	□
Fe III, Fe II	1623–1637	1615–1623, 1643–1648	★

^aIn Figs. 9 and 11.

Table 7: Absorption Lines

Feature	λ_o	M 60		NGC 3379		Model
		EW(\AA) ^a	Significance	EW (\AA) ^a	Significance	EW(\AA) ^b
Ly δ	949.8	2.2 ± 0.5	7.1×10^{-7}	2.5 ± 0.7	4.1×10^{-1}	3.8
Ly γ	972.9	3.2 ± 0.6	3.9×10^{-8}	2.4 ± 0.5	1.1×10^{-1}	6.8
C III	977.2	1.4 ± 0.6	7.6×10^{-1}	2.8 ± 0.5	7.2×10^{-1}	1.6
N III	991.7	< 1.5	-	0.8 ± 1.1	9.2×10^{-1}	0.8
Ly β	1026.0	10.6 ± 0.4	$< 10^{-10}$	8.9 ± 0.4	2.0×10^{-6}	12.7
C II	1036.4	1.1 ± 0.4	2.8×10^{-1}	0.3 ± 0.6	1.0×10^0	1.5
N II	1085.3	1.5 ± 0.4	3.2×10^{-4}	0.9 ± 0.7	8.0×10^{-1}	0.8
C III	1175.8	1.3 ± 0.4	3.0×10^{-3}	2.2 ± 0.7	8.2×10^{-2}	0.8
Si II	1263.0	< 1.0	-	< 2.7	-	1.4
C II	1335.2	0.6 ± 0.3	5.5×10^{-1}	< 2.5	-	0.6
Si IV	1394.1	1.1 ± 1.1	8.7×10^{-2}	0.3 ± 0.4	0.99×10^{-1}	0.3
Si IV	1402.5	1.2 ± 0.6	6.5×10^{-2}	< 2.0	-	0.1
C IV	1550.2	< 1.4	-	< 2.7	-	0.2

^aUncertainties are from the 1σ errors, and upper limits are for the 2σ confidence level.

^bBest fit EHB + PAGB model for M 60, with $Z_{atm} = 0.1 Z_{\odot}$.